CAPITAL UNIVERSITY OF SCIENCE AND
TECHNOLOGY, ISLAMABAD

Attenuation Performance with Lined Expansion Chambers

by

Muhammad Hafeez

A thesis submitted in partial fulfillment for the
degree of Master of Philosophy

in the

Faculty of Computing
Department of Mathematics

2019

I dedicate this humble work to my beloved parents.

For their endless love, support, encouragement and prayers.

CERTIFICATE OF APPROVAL

Attenuation Performance with Lined Expansion Chambers

by

Muhammad Hafeez

(MMT163019)

THESIS EXAMINING COMMITTEE

S. No.	Examiner	Name	Organization
(a)	External Examiner	Dr. Mahmood ul Hassan	COMSATS, Islamabad
(b)	Internal Examiner	Dr. Abdul Rehman Kashif	CUST, Islamabad
(c)	Supervisor	Dr. Muhammad Afzal	CUST, Islamabad

Dr. Muhammad Afzal
Thesis Supervisor
December, 2019

Dr. Muhammad Sagheer
Head
Dept. of Mathematics
December, 2019

Dr. Muhammad Abdul Qadir
Dean
Faculty of Computing
December, 2019

Author's Declaration

I, **Muhammad Hafeez** hereby state that my M.Phil thesis titled "**Attenuation Performance with Lined Expansion Chambers**" is my own work and has not been submitted previously by me for taking any degree from Capital University of Science and Technology, Islamabad or anywhere else in the country/abroad.

At any time if my statement is found to be incorrect even after my graduation, the University has the right to withdraw my M.Phil Degree.

(Muhammad Hafeez)
Registration No: MMT163019

Plagiarism Undertaking

I solemnly declare that research work presented in this thesis titled "**Attenuation Performance with Lined Expansion Chambers**" is solely my research work with no significant contribution from any other person. Small contribution/help wherever taken has been duly acknowledged and that complete thesis has been written by me.

I understand the zero tolerance policy of the HEC and Capital University of Science and Technology towards plagiarism. Therefore, I as an author of the above titled thesis declare that no portion of my thesis has been plagiarized and any material used as reference is properly referred/cited.

I undertake that if I am found guilty of any formal plagiarism in the above titled thesis even after award of M.Phil Degree, the University reserves the right to withdraw/revoke my M.Phil degree and that HEC and the University have the right to publish my name on the HEC/University website on which names of students are placed who submitted plagiarized work.

(Muhammad Hafeez)
Registration No: MMT163019

Acknowledgements

In the name of **ALLAH**, the most Beneficent and the most Merciful. All praises to **ALLAH**, Who taught (the use of) the pen, taught man that which he knew not. I bear witness that **MUHAMMAD (PBUH)** is the last prophet of **ALLAH**, Whose life is a perfect model for all mankind till the final day.

I submit my heartiest gratitude to my respected supervisor **Dr. Muhammad Afzal**, the Assistant professor of Mathematics in CUST, for his sincere guidance for completing this thesis.

I am also deeply indebted to my respected HOD, **Dr. Muhammad Saghir** and other respected faculty members of Mathematics department for their invaluable help during study.

I humbly extend my thanks to all colleagues for their valuable support during research.

Finally, I sincerely thank to my parents, my brothers, my sister, my nephews, cousins and other family members for their encouragement, moral support, care and prayers.

(Muhammad Hafeez)

Registration No: MMT163019

Abstract

The attenuation of acoustic waves with lined expansion chambers is presented. The physical problems involve scattering and absorption of acoustic waves in waveguide including single as well as double expansion chambers. The Mode Matching technique is used to solve the governing boundary value problems. The technique is based on the determination of eigenfunction expansions of duct regions through separation of variable method. The matching of pressures and velocities modes at interfaces help to reconstruct the differentiated system into linear algebraic systems. These systems are truncated and solved numerically. To insight the problems physically the transmission loss is plotted against frequency. It is found that more attenuation with double lined expansion chambers and fibrous material is obtained.

Contents

List of Figures

Chapter 1

Introduction

Noise pollution is the biggest problem of modern era. It not only disrupts the normal functioning of life but also affects the health of humans. The major effects of noise on humans include: physiological effects, increase of blood pressure and feeling of headache; psychological effects, stress and nervousness and social effects, obstruction of communication and social segregation. The main sources of noise are road traffic, airplanes, railways, construction sites and industrial areas. In order to reduce the unwanted noise various noise control measures are used. For example silencers like components are employed at the exhausts of automobiles. The inside of these silencers involve various geometric designs and sound absorbing materials that minimize the vibrational waves of exhaust engines and fans. Moreover for the noise of Heating, Ventilation and Air Conditioning (HVAC) systems of building, different duct designs and sound proofing are used. The common component in all is the duct like structures. It works like a channel which transports vibrational energy from one point of the medium to another point. The investigation on designs and materials properties of such ducts in order to minimize the vibrational energy has gained much attention of researcher and engineers. The current study is relevant to the propagation and attenuation of sound radiation in a waveguide including single and double cavities or expansion chambers. The material properties of bounding regions of chambers contain porous linings. Such waveguides may have applications in HVAC and silencer designs.

In this thesis the modeling of acoustic duct modes, their propagation, scattering and absorption are discussed.

1.1 Background and Literature Survey

The word acoustic is as old as human history. In the 6th century BC, Pythagoras gave the idea of musical sounds and vibrating strings. He found that consonant musical intervals produced by the vibrating strings depend upon tension of string. The Roman architect Vitruvius worked on the designs of acoustical theaters. Galileo discussed about the relationship of pitch of a vibrating string to its length. Sauveur made complete study about the relationship of frequency to pitch. The English mathematician Taylor formulated the fundamental mode solution to investigate the vibration of string with reference to the frequency of propagating mode. Bernoulli provided partial differential equation for the vibrating string and obtained its solution through d'Alembert principle. Poisson discussed first time the solution of vibrational membranes. Clebsch presented solution for vibrating circular membranes. Chladni formulated the solution of vibrating plates.

In the 19th century, Tyndall observed that longitudinal vibration was produced by rubbing a rod. He also formulated the effects of fog and water in various weather conditions on the transmission of sound. Helmholtz improved the work of Tyndall by working over the quality of musical sound and invented a vibrational microscope. Stokes presented a three-dimensional equation of motion of a viscous fluid which was known as Navier-Stokes equation. Bell invented a microphone. Edison recorded first time human voice for posterity. Scheibler formed tonometer which controlled the frequency in small steps. Koenig formed a tonometer which controlled frequency ranging from 16Hz to 21845Hz. Koenig made cylindrical and spherical Helmholtz resonators of different kinds.

In 20th century, Sabine, father of architectural acoustics, measured quantity of sound in the room and made acoustical theaters. Rayleigh found a way to measure the intensity of a sound source. Knudsen and Harris improved the work of Sabine by investigating the effects of molecular relaxation phenomena in gases

and liquid. Bolt with the help of Beranek and Newman worked over the acoustical building, halls, musical sheds and centers for performing art. Lighthill studied about non-linear acoustics in fluid. Hamilton, Blackstock and Beyer investigated the propagation of sound through liquids, gases or solids.

The present study is related to the propagation and scattering of acoustics waves in rectangular waveguide or channel. The performance of acoustical waveguide to reduce unwanted noise can be increased by using the noise absorbent material and/or introducing the locally reactive liners.

The salient features of acoustics scattering in guiding structures that contain expansions and/or contractions in geometry have vital role in noise reduction applications. For example, expansion chambers are widely used to reduce unwanted exhaust noise produced by internal combustion engines that travels through the duct. The propagation of wave along the ducts with rapid changes in the cross sectional area can produce reflections that reduce the energy of transmitted wave. This is the method together with cavity resonance mechanisms by which silencer box reduce noise in the car exhaust system [1].

Hassan and Rawlins [2], Rawlins [3, 4] and Ayub et al [5–7] discussed the propagation of sound waves in cylinderical channel containing sound absorbing linings along the walls of the channel. They used Wiener Hopf technique to analyze the effects of absorbing material.

Recently Haung [8] and then Haung and Choy [9] investigated different aspects of channels for distortion of fan noise in HVAC system. They used geometrical channels containing elastic membranes and employed Fourier integral based matching approach for the solution of their problem. Lawrie [10] presented the class of orthogonality relations relevant to fluid-structure interaction. Haung [11] analyzed drum like silencer and reflection of sound waves through chamber enclosed by vertical plates.

More recently, in references [12–23] the Mode Matching technique have been used and advanced for the problems of Sturm-Liouville systems and non Sturm Liouville systems catagories.

The present work is geometrical extended form of the work done by Demir and

Buyukaksoy [24]. They considered circular single expansion chamber whose walls containing reacting linings of porous material. Here, we considered rectangular single and double expansion chambers in waveguides with different bounding properties. The Mode Matching approach has been used to found the solution of governing BVP.

The thesis is organized as follow:

In Chapter 1 the introduction and literature survey is presented. Chapter 2 contains some basic definitions and terminologies. The mathematical formulation of waveguides involving single expansion chamber is discussed in Chapter 3, whereas, the analysis of waveguides with double expansion chambers are debated in Chapter 4. In Chapter 5 discussion and conclusion are presented.

Chapter 2

Preliminaries

2.1 Acoustics

Acoustics is an old discipline of science that deals with the study of sound. The word acoustics is derived from a Greek letter "akouein", which means "to hear". The word "acoustics" was first time used by Sauveur in 1701. But now it is a branch of physics and covers many important disciplines like theoretical acoustics, nonlinear acoustics, underwater acoustics, ultrasound, vibrations, noise control, room acoustics, building acoustics, electric acoustics, and acoustics of the ear.

2.2 Acoustic Waves

Acoustic waves are the pressure fluctuations in a material medium which transfer energy from one medium to another medium. This medium can be a compressible fluid like gases(air) or liquid(water) or any other vibrating systems.

2.3 Acoustic Wave Equation

In order to derive the acoustic wave equation in compressible fluid (air), we use some basic laws, which are given as follows:

Conservation of mass: The conservation of mass is described by the partial differential equation as:

$$\frac{\partial \rho}{\partial t^*} + \nabla^* \cdot \rho u^* = 0, \tag{2.1}$$

where ρ is density and u represents velocity vector.

Conservation of momentum: The conservation of momentum is described as:

$$\rho \left(\frac{\partial u^*}{\partial t^*} + (u^* \cdot \nabla^*) u^* \right) = -\nabla^* p + \rho g^*, \tag{2.2}$$

where p is acoustic pressure and g is gravitational acceleration.

Equation of state: The equation of state for acoustic wave equation is written as:

$$p = \beta s, \tag{2.3}$$

where β is bulk modulus and s represents condensation.

By using aforementioned laws, we can obtain linearized acoustic wave equation.

$$\nabla^{*2} p = \frac{1}{c^2} \frac{\partial^2 p}{\partial t^{*2}}, \tag{2.4}$$

where

$$c^2 = \frac{\beta}{\rho_0}, \quad u^* = \nabla^* \Phi, \quad p = -\rho_o \frac{\partial \Phi}{\partial t^*}. \tag{2.5}$$

We can write acoustic wave equation in terms of scalar field potential as:

$$\nabla^{*2} \Phi = \frac{1}{c^2} \frac{\partial^2 \Phi}{\partial t^{*2}}, \tag{2.6}$$

where Φ represents field potential.

The equation (2.6) is used to discuss the wave propagation in fluids.

2.4 Boundary Conditions

The following boundary conditions are defined to model the BVP:

1) Soft conditions.

2) Rigid conditions.

3) Impedance conditions.

2.4.1 Soft Conditions

The soft boundary conditions are Drichlet's type boundary conditions. For this condition, the pressure or displacement is assumed as zero, i.e.

$$\phi(x, y) = 0. \tag{2.7}$$

2.4.2 Rigid Conditions

The rigid boundary conditions are Neumann's type boundary conditions. For this condition, normal velocity is assumed as zero, i.e.

$$\frac{\partial \phi(x, y)}{\partial y} = 0. \tag{2.8}$$

2.4.3 Impedance Conditions

The impedance boundary conditions are Robin's type boundary conditions. Robin boundary conditions are combination of Drichlet boundary conditions and Neumann boundary conditions. This condition is written as:

$$a_1 \phi_(x, y) + a_2 \frac{\partial \phi(x, y)}{\partial y} = 0, \tag{2.9}$$

where a_1 and a_2 are arbitrary constants.

2.5 Energy Flux

For fluid potential ϕ the energy flux may be defined by [25]:

$$\text{Energy Flux} = \frac{1}{2} Re \left[i \int_{\Omega} \phi \left(\frac{\partial \phi}{\partial \mathbf{n}} \right)^{\star} d\Omega \right], \tag{2.10}$$

where $\mathbf{n}$ is normal to the given region and $(\star)$ is the complex conjugate.

To measure the performance of the dissipative silencer the transmission loss is defined by[26]

$$TL = -10 \log_{10} \left(\frac{P_{tr}}{P_{inc}} \right), \tag{2.11}$$

where P_{tr} and P_{inc} show the transmitted power (out going energy flux) and incident power (in coming incident energy flux).

Chapter 3

Scattering in Waveguide Involving Single Expansion Chamber

In this chapter we consider the propagation and scattering of acoustic wave through an expansion chamber including absorbing lining in a waveguide. The governing boundary value problem (BVP) involve Helmholtz equation along with rigid and impedance type boundary conditions. The Mode-Matching technique has been used to solve the BVP. The mathematical formulation and solution procedure is discussed comprehensively in next sections 3.1-3.4. The section wise detail is given as follows: In section 3.1 the mathematical formulation of the boundary value problem is given. In section 3.2 mode matching solution of the boundary value problem is discussed. In section 3.3 the derivation of energy flux is given. In section 3.4 the numerical results and discussion are provided.

3.1 Mathematical Formulation

Consider a two dimensional waveguide stretched infinitely along x^*-direction and contains finite height along y^*-direction, where asterisk here and henceforth denotes the dimensional quantity. Moreover, the waveguide comprises step-discontin uities at $x^* = \pm L^*$ that divide the waveguide into ducts of different heights. Two side ducts of same heights occupy the regions at $\mid x^* \mid > L^*$, $\mid y^* \mid < a^*$ and one central region $\mid x^* \mid < L^*$ and $\mid y^* \mid < b^*$. The interior of the waveguide is filled with compressible fluid of density ρ and sound speed c, whilst, the outer side is in vacau. The horizontal boundaries of side regions at $y^* = \pm a^*$ are rigid whereas the horizontal boundaries of central region contain absorbing lining. The vertical boundaries at $x^* = \pm L^*$ can be of two different categories:

1) Rigid vertical strips.

2) Porous linings along the vertical strips.

The physical configuration of the waveguide for rigid vertical strips is shown in Figure 3.1. Now let a harmonic time dependent plane acoustic wave propagat-

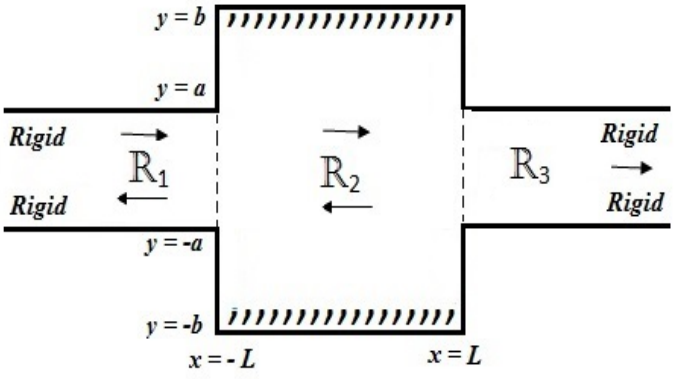

FIGURE 3.1: Geometry of the problem.

ing from negative x^*-direction towards $\mid x^* \mid \leqslant L^*$. At $\mid x^* \mid \leqslant L^*$, it will scatter into infinite number of reflected and transmitted modes. The dimensional fluid potential $\Phi^*(x^*, y^*, t^*)$ satisfy the linear acoustic wave equation,

$$\frac{\partial^2 \Phi^*}{\partial x^{*2}} + \frac{\partial^2 \Phi^*}{\partial y^{*2}} = \frac{1}{c^2} \frac{\partial^2 \Phi^*}{\partial t^{*2}}. \tag{3.1}$$

On taking the harmonic time dependence of $e^{-i\omega t^*}$, where ω is the circular frequency, the dimensional field potential can be written as:

$$\Phi^*(x^*, y^*, t^*) = \phi^*(x^*, y^*)e^{-i\omega t^*}, \tag{3.2}$$

where $\phi^*(x^*, y^*)$ is the time independent dimensional field potential. On using (3.2) into (3.1) we get the Helmholtz equation

$$(\frac{\partial^2}{\partial x^{*2}} + \frac{\partial^2}{\partial y^{*2}} + k^2)\phi^*(x^*, y^*) = 0, \tag{3.3}$$

with $k = \omega/c$ the dimensional wave number. The dimensional length and time are made dimensionless by using the transformations,

$$x = kx^*, \quad y = ky^* \quad and \quad t = \omega t^*, \tag{3.4}$$

where k^{-1} and ω^{-1} are assumed to contain length and time scale, respectively. Therefore we may write

$$\frac{\partial}{\partial x^*} = k\frac{\partial}{\partial x}, \tag{3.5}$$

$$\frac{\partial^2}{\partial x^{*2}} = k^2\frac{\partial^2}{\partial x^2}, \quad \frac{\partial^2}{\partial y^{*2}} = k^2\frac{\partial^2}{\partial y^2} \tag{3.6}$$

and

$$\Phi^*(x^*, y^*) = \frac{1}{k^2}\phi(x, y). \tag{3.7}$$

By using (3.6) and (3.7) into (3.3) we found the non-dimensional form of Helmholtz equation

$$(\frac{\partial^2}{\partial x^2} + \frac{\partial^2}{\partial y^2} + 1)\phi(x, y) = 0, \tag{3.8}$$

where $\phi(x, y)$ is the dimensionless form of fluid potential.

With reference to different duct regions, this field potential can be written as:

$$\phi\,(x, y) = \begin{cases} \phi_1\,(x, y)\,, & x < -L, \quad \mid y \mid < a, \\ \phi_2\,(x, y)\,, & \mid x \mid < L, \qquad y < b. \\ \phi_3\,(x, y)\,, & x > L, \quad \mid y \mid < a. \end{cases} \tag{3.9}$$

The dimensionless form of boundary conditions can be written as:

$$\frac{\partial \phi_1}{\partial y} = 0, \qquad x < -L, \quad y = \pm a, \tag{3.10}$$

$$\phi_2 \pm i\xi \frac{\partial \phi_2}{\partial y} = 0, \quad \mid x \mid < L, \quad y = \pm b \tag{3.11}$$

and

$$\frac{\partial \phi_3}{\partial y} = 0, \qquad x > L, \quad y = \pm a. \tag{3.12}$$

The boundaries along the vertical strips can be rigid or absorbing lining. The rigid vertical boundaries (shown in Figure 3.1) are

$$\frac{\partial \phi_2}{\partial x} = 0, \qquad y = \pm L, \quad a \leqslant x \leqslant b. \tag{3.13}$$

The vertical absorbing lining boundaries (shown in Figure 3.2) are given by

$$\phi_2 \mp i\xi \frac{\partial \phi_2}{\partial x} = 0, \quad y = \pm L, \quad a \leqslant x \leqslant b. \tag{3.14}$$

In next section the boundary value problem is solved by using Mode-Matching technique.

3.2 Mode Matching Solution

Here we find the Mode Matching solution of the boundary value problem formulated in section 3.1. Consider a plane wave incident ϕ_{inc} which is a fundamental duct mode of region $x < -L$, is propagating from negative x-direction towards $\mid x \mid \leqslant L$. The field potential $\phi_1(x, y)$ in duct region $x < -L$ is the sum of incident and reflected fields, that is:

$$\phi_1(x, y) = \phi_{inc} + \phi_{ref}, \tag{3.15}$$

here, ϕ_{ref} is the infinite sum of reflected duct modes that is

$$\phi_{ref} = \sum_{n=0}^{\infty} A_n \phi_{1n}(x, y), \tag{3.16}$$

where A_n, $n = 0, 1, 2, ...$ are the amplitudes of reflected modes. To calculate the n^{th} reflected duct mode $\phi_{1n}(x, y)$, n = 0, 1, 2, ... we use the method of separation of variables. For this let

$$\phi_{1n}(x, y) = X_{1n}(x) Y_{1n}(y). \tag{3.17}$$

We use (3.17) into (3.8) to get

$$-\left(\frac{Y_{1n}''}{Y_{1n}} + 1\right) = \frac{X_{1n}''}{X_{1n}} = -\eta_n^2. \tag{3.18}$$

In above equation prime denotes the differentiation with respect to the variable involved. Now on solving for $X_{1n}(x)$ and $Y_{1n}(y)$, we may find

$$X_{1n}(x) = C_1 e^{-i\eta_n(x+L)} + C_2 e^{+i\eta_n(x+L)} \tag{3.19}$$

and

$$Y_{1n}(y) = C_3 \cos(\tau_n y) + C_4 \sin(\tau_n y), \tag{3.20}$$

where $\eta_n = \sqrt{1 - \tau_n^2}$, $n = 0, 1, 2, \ldots$ are the wave number of propagating modes. Note that $X_{1n}(x)$ determines the shape of n^{th} mode propagating in R_1 along x-direction. The exponential term $\exp -i\eta_n(x + L)$ in (3.19) indicates the n^{th} mode propagating towards negative x-direction while $\exp +i\eta_n(x+L)$ show the n^{th} mode propagating towards positive x-direction. As the reflected n^{th} mode propagates in negative x-direction, so $C_2 = 0$. Also applying the rigid boundary condition (3.10) we found $C_4 = 0$ and $\tau_n = n\pi/2a$, $n = 0, 1, 2, ...$ Therefore, the reflected field can be written as:

$$\phi_{ref} = \sum_{n=0}^{\infty} A_n \cos\{\frac{n\pi}{2a}(y + a)\} e^{-i\eta_n(x+L)}. \tag{3.21}$$

On assuming the incident wave to be the fundamental duct mode, the field potential in region R_1 can be written as

$$\phi_1(x,y) = e^{i(x+L)} + \sum_{n=0}^{\infty} A_n \cos\{\frac{n\pi}{2a}(y+a)\}e^{-i\eta_n(x+L)}. \tag{3.22}$$

Note that the first term in (3.22) stands for incident field which is a fundamental duct mode $n = 0$ propagating towards positive x-direction, while the second term is the reflected field. Similarly for region R_2, the eigen expansion form of reflected and transmitted duct mode are assumed as:

$$\phi_2(x,y) = \sum_{n=0}^{\infty} \phi_{2n}(x,y), \tag{3.23}$$

where $\phi_{2n}(x,y)$ denotes the n^{th} propagating modes. To find $\phi_{2n}(x,y)$ from the boundary conditions of R_2, we use method of separation of variables. For this, we assume

$$\phi_{2n}(x,y) = X_{2n}(x)Y_{2n}(y). \tag{3.24}$$

By using (3.24) into (3.8), we found

$$-\left(\frac{Y_{2n}''}{Y_{2n}} + 1\right) = \frac{X_{2n}''}{X_{2n}} = -\nu_n^2, \tag{3.25}$$

which implies

$$X_{2n}(x) = C_5 e^{+i\nu_n x} + C_6 e^{-i\nu_n x} \tag{3.26}$$

and

$$Y_{2n}(y) = C_7 \cos(\gamma_n y) + C_8 \sin(\gamma_n y), \tag{3.27}$$

where $\nu_n = \sqrt{1-\gamma_n^2}$ is the wave number of the propagating n^{th} mode. On using (3.27) into (3.11), we get the eigenfunction in R_2 as:

$$Y_n(y) = \sin\gamma_n(y+b) + i\xi_n\gamma_n \cos\gamma_n(y+b), \tag{3.28}$$

where γ_n, $n = 0, 1, 2, ...$ the eigen values are the roots of characteristic equation:

$$\sin\gamma_n(2b) + 2i\xi_n\gamma_n\cos(2\gamma_n b) + \xi_n^2\gamma_n^2\sin(2\gamma_n b) = 0. \tag{3.29}$$

These roots can be found numerically. Hence the reflected and transmitted field in R_2 can be written as:

$$\phi_2(x, y) = \sum_{n=0}^{\infty}\{B_n e^{i\nu_n x} + C_n e^{-i\nu_n x}\}Y_n(y), \tag{3.30}$$

where B_n and C_n, $n = 0, 1, 2, ...$ are the amplitudes of n^{th} transmitted and reflected mode in R_2, respectively. Likewise we obtain the eigenfunction expansion form in region R_3 as:

$$\phi_3(x, y) = \sum_{n=0}^{\infty} D_n\cos\{\frac{n\pi}{2a}(y + a)\}e^{+i\eta_n(x-L)}, \tag{3.31}$$

where coefficient D_n, $n = 0, 1, 2, ...$ are the amplitude of n^{th} transmitted duct modes in R_3. Note in (3.22), (3.30) and (3.31) the modal coefficient $\{A_n, B_n, C_n, D_n\}$, $n = 0, 1, 2, ...$ are unknowns. To determine these unknowns we use the matching procedure. Now it is convenient to match the pressures and normal velocities at $x = \pm L$. From the continuity of pressures, we have

$$\phi_1(-L, y) = \phi_2(-L, y), \quad -a \leqslant y \leqslant a \tag{3.32}$$

and

$$\phi_3(L, y) = \phi_2(L, y), \qquad -a \leqslant y \leqslant a. \tag{3.33}$$

Using (3.22) and (3.30) into continuity condition of pressure (3.32), we obtain

$$1 + \sum_{n=0}^{\infty} A_n\cos\{\frac{n\pi}{2a}(y + a)\} = \sum_{n=0}^{\infty}\{B_n e^{-i\nu_n L} + C_n e^{i\nu_n L}\}Y_n(y). \tag{3.34}$$

On multiplying (3.34) with $\cos\{\frac{m\pi}{2a}(y+a)\}$ and integrating with respect to y over $-a \leqslant y \leqslant a$, we found

$$\int_{-a}^{a} \cos\{\frac{m\pi}{2a}(y+a)\}dy + \sum_{n=0}^{\infty} A_n \int_{-a}^{a} \cos\{\frac{m\pi}{2a}(y+a)\}\cos\{\frac{n\pi}{2a}(y+a)\}dy$$
$$= \sum_{n=0}^{\infty}\{B_n e^{-i\nu_n L} + C_n e^{i\nu_n L}\}\int_{-a}^{a} \cos\{\frac{m\pi}{2a}(y+a)\}Y_n(y)dy. \tag{3.35}$$

As the eigen functions $\cos\{\frac{m\pi}{2a}(y+a)\}$, m = 0, 1, 2,... are orthogonal in nature, which satisfy the usual orthogonal relation

$$\int_{-a}^{a} \cos\{\frac{m\pi}{2a}(y+a)\}\cos\{\frac{n\pi}{2a}(y+a)\}dy = a\delta_{mn}\epsilon_m, \tag{3.36}$$

where δ_{mn} is the kronecker delta and

$$\epsilon_m = \begin{cases} 2, & m = 0, \\ 1, & \text{otherwise.} \end{cases} \tag{3.37}$$

By using (3.36) and (3.37) into (3.35), we get

$$A_m = -\delta_{m0} + \frac{1}{\epsilon_m a}\sum_{n=0}^{\infty}\{B_n e^{-i\nu_n L} + C_n e^{i\nu_n L}\}R_{mn}, \tag{3.38}$$

where

$$R_{mn} = \int_{-a}^{a} \cos\{\frac{m\pi}{2a}(y+a)\}Y_n(y)dy. \tag{3.39}$$

Also on using (3.30) and (3.31) into continuity condition of pressure (3.33), we obtain

$$\sum_{n=0}^{\infty} D_n \cos\{\frac{n\pi}{2a}(y+a)\} = \sum_{n=0}^{\infty}\{B_n e^{i\nu_n L} + C_n e^{-i\nu_n L}\}Y_n(y). \tag{3.40}$$

On multiplying (3.40) with $\cos\{\frac{m\pi}{2a}(y+a)\}$ and integrating with respect to y over$-a \leqslant y \leqslant a$, we have

$$\sum_{n=0}^{\infty} D_n \int_{-a}^{a} \cos\{\frac{m\pi}{2a}(y+a)\}\cos\{\frac{n\pi}{2a}(y+a)\}dy =$$
$$\sum_{n=0}^{\infty}\{B_n e^{i\nu_n L} + C_n e^{-i\nu_n L}\}\int_{-a}^{a}\cos\{\frac{m\pi}{2a}(y+a)\}Y_n(y)dy. \tag{3.41}$$

On substituting (3.36) and (3.37) into (3.41), we get

$$D_m = \frac{1}{a\epsilon_m}\sum_{n=0}^{\infty}\{B_n e^{-i\nu_n L} + C_n e^{i\nu_n L}\}R_{mn}. \tag{3.42}$$

By adding (3.38) and (3.42), we found

$$\Psi_m^+ = -\delta_{m0} + \frac{2}{\epsilon_m a}\sum_{n=0}^{\infty} L_n^+ \cos(\nu_n L)R_{mn}. \tag{3.43}$$

And by subtracting (3.38) and (3.42), we have

$$\Psi_m^- = -\delta_{m0} - \frac{2i}{\epsilon_m a}\sum_{n=0}^{\infty} L_n^- \sin(\nu_n L)R_{mn}, \tag{3.44}$$

where $\Psi_m^{\pm} = (A_m \pm D_m)$ and $L_n^{\pm} = (B_n \pm C_n)$. Here we discuss the two categories of the above problem.

3.2.1 Rigid Vertical Strips

For rigid vertical strips of the expansion chamber the continuity conditions of normal velocities are defined by

$$\phi_{2x}(-L,y) = \begin{cases} 0, & -b \leqslant y \leqslant -a, \\ \phi_{1x}(-L,y), & -a \leqslant y \leqslant a, \\ 0, & a \leqslant y \leqslant b \end{cases} \tag{3.45}$$

and

$$\phi_{2x}(L,y) = \begin{cases} 0, & -b \leqslant y \leqslant -a, \\ \phi_{3x}(L,y), & -a \leqslant y \leqslant a, \\ 0, & a \leqslant y \leqslant b. \end{cases} \tag{3.46}$$

On using (3.22) and (3.30) into the condition of normal velocity (3.45), we found that

$$i\sum_{n=0}^{\infty}\{B_n e^{-i\nu_n L} - C_n e^{i\nu_n L}\}\nu_n Y_n(y) =$$
$$\begin{cases} 0, & -b \leqslant y \leqslant -a, \\ i - i\sum_{n=0}^{\infty} A_n\eta_n \cos\{\frac{n\pi}{2a}(y+a)\}, & -a \leqslant y \leqslant a, \\ 0, & a \leqslant y \leqslant b. \end{cases} \tag{3.47}$$

We multiply (3.47) by $Y_m(y)$ and then integrate with respect to y over $-b \leqslant y \leqslant b$, we obtain

$$i\sum_{n=0}^{\infty}\{B_n e^{-i\nu_n L} - C_n e^{i\nu_n L}\}\nu_n \int_{-b}^{b} Y_m(y)Y_n(y)dy =$$
$$i\int_{-a}^{a} Y_m(y)dy - i\sum_{n=0}^{\infty} A_n\eta_n \int_{-a}^{a} Y_m(y)\cos\{\frac{n\pi}{2a}(y+a)\}dy. \tag{3.48}$$

As the eigenfunctions $Y_m(y)$, m = 0, 1, 2,..., satisfy the dispersion relations

$$\int_{-b}^{b} Y_n(y)Y_m(y)dy = E_m\delta_{mn} \tag{3.49}$$

and

$$E_m = \int_{-b}^{b} Y_m^2(y)dy. \tag{3.50}$$

Using (3.49) and (3.50) into (3.48), we have

$$B_m e^{-i\nu_m L} - C_m e^{i\nu_m L} = \frac{R_{0m}}{E_m\nu_m} - \frac{1}{E_m\nu_m}\sum_{n=0}^{\infty} A_n\eta_n R_{nm}. \tag{3.51}$$

Similarly, on using (3.30) and (3.31) into the condition of normal velocity (3.46), we get

$$i\sum_{n=0}^{\infty}\{B_n e^{i\nu_n L} - C_n e^{-i\nu_n L}\}\nu_n Y_n(y) =$$
$$\begin{cases} 0, & -b \leqslant y \leqslant -a, \\ i\sum_{n=0}^{\infty} D_n\eta_n \cos\{\dfrac{n\pi}{2a}(y+a)\}, & -a \leqslant y \leqslant a, \\ 0, & a \leqslant y \leqslant b. \end{cases} \tag{3.52}$$

By multiplying (3.52) by $Y_m(y)$ and then integrating with respect to y over $-a \leqslant y \leqslant a$, we obtain

$$\begin{aligned} & i\sum_{n=0}^{\infty}\{B_n e^{i\nu_n L} - C_n e^{-i\nu_n L}\}\nu_n \int_{-a}^{a} Y_m(y)Y_n(y)dy \\ &= i\sum_{n=0}^{\infty} D_n\eta_n \int_{-a}^{a} Y_m(y)\cos\{\frac{n\pi}{2a}(y+a)\}dy. \end{aligned} \tag{3.53}$$

Using (3.49) and (3.50) into (3.53), we have

$$B_m e^{i\nu_m L} - C_m e^{-i\nu_m L} = \frac{1}{E_m\nu_m}\sum_{n=0}^{\infty} D_n\eta_n R_{nm}. \tag{3.54}$$

Also adding (3.51) and (3.54), we get

$$L_m^- = \frac{R_{0m}}{2\cos(\nu_m L)E_m\nu_m} - \frac{1}{2\cos(\nu_m L)E_m\nu_m}\sum_{n=0}^{\infty}\Psi_n^-\eta_n R_{nm}. \tag{3.55}$$

On subtracting (3.51) and (3.54), we found

$$L_m^+ = \frac{-R_{0m}}{2i\sin(\nu_m L)E_m\nu_m} + \frac{1}{2i\sin(\nu_m L)E_m\nu_m}\sum_{n=0}^{\infty}\Psi_n^+\eta_n R_{nm}, \tag{3.56}$$

where $\Psi_n^{\pm} = (A_n \pm D_n)$ and $L_m^{\pm} = (B_m \pm C_m)$.

In this way we get a system of equations defined by (3.43) and (3.56) with unknowns L_m^+ and Ψ_m^+. Likewise a system for unknowns L_m^- and Ψ_m^- is given in (3.44) and (3.55). These systems are truncated and solved numerically for $L_m^{\pm}$ and $\Psi_m^{\pm}$.

Then the model amplitudes $\{A_m, B_m, C_m, D_m\}$ are found from these values $L_m^{\pm}$ and $\Psi_m^{\pm}$ as:

$$A_m = \frac{\Psi_m^+ + \Psi_m^-}{2}, \quad D_m = \frac{\Psi_m^+ - \Psi_m^-}{2}$$

and

$$B_m = \frac{L_m^+ + L_m^-}{2}, \quad C_m = \frac{L_m^+ - L_m^-}{2}.$$

3.2.2 Porous Linings along the Vertical Strips

This waveguide is extension of previous duct cavity system. In this waveguide, we will discuss the expansion chamber with horizontal and vertical absorbing lining. The governing boundary value problem for this waveguide is obtained by inserting vertical absorbing lining in region R_2. The geometrical configuration for porous linings along the vertical strips is shown in Figure 3.2.

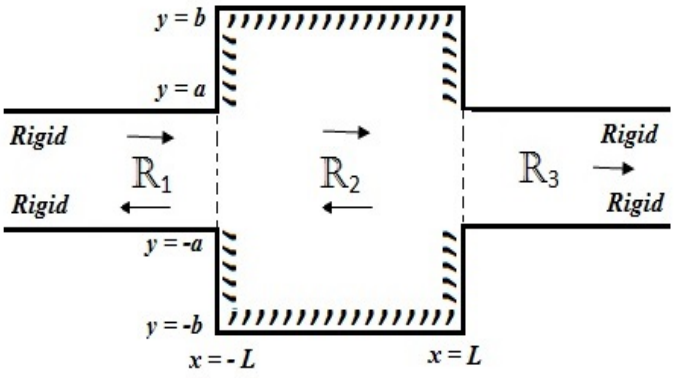

FIGURE 3.2: Geometry of the problem.

For porous linings along the vertical strips of the expansion chamber the continuity conditions of normal velocities are defined by

$$\phi_{2x}(-L, y) = \begin{cases} \phi_{1x}(-L, y), & -a \leqslant y \leqslant a, \\ \dfrac{-i}{\xi}\phi_2(-L, y), & a \leqslant y \leqslant b, \\ \dfrac{-i}{\xi}\phi_2(-L, y), & -b \leqslant y \leqslant -a \end{cases} \tag{3.57}$$

and

$$\phi_{2x}(L,y)=\begin{cases}\dfrac{i}{\xi}\phi_2(L,y), & a\leqslant y\leqslant b,\\ \phi_{3x}(L,y), & -a\leqslant y\leqslant a,\\ \dfrac{i}{\xi}\phi_2(L,y), & -b\leqslant y\leqslant -a.\end{cases}\tag{3.58}$$

Using (3.22) and (3.30) into the condition of normal velocity (3.57), we found that

$$\begin{aligned}&i\sum_{n=0}^{\infty}\{B_ne^{-i\nu_nL}-C_ne^{i\nu_nL}\}\nu_nY_n(y)=\\ &\begin{cases}i-i\sum_{n=0}^{\infty}A_n\eta_n\cos\{\dfrac{n\pi}{2a}(y+a)\}, & -a\leqslant y\leqslant a,\\ \dfrac{-i}{\xi}\sum_{n=0}^{\infty}\{B_ne^{-i\nu_nL}+C_ne^{i\nu_nL}\}Y_n(y), & a\leqslant y\leqslant b,\\ \dfrac{-i}{\xi}\sum_{n=0}^{\infty}\{B_ne^{-i\nu_nL}+C_ne^{i\nu_nL}\}Y_n(y), & -b\leqslant y\leqslant -a.\end{cases}\end{aligned}\tag{3.59}$$

We multiply (3.59) by $Y_m(y)$ and then integrate with respect to y over $-b\leqslant y\leqslant b$ to achieve

$$\begin{aligned}&i\sum_{n=0}^{\infty}\{B_ne^{-i\nu_nL}-C_ne^{i\nu_nL}\}\nu_n\int_{-b}^{b}Y_m(y)Y_n(y)dy\\ &=i\int_{-a}^{a}Y_m(y)dy-i\sum_{n=0}^{\infty}A_n\eta_n\int_{-a}^{a}Y_m(y)\cos\{\frac{n\pi}{2a}(y+a)\}dy\\ &\quad-\frac{i}{\xi}\sum_{n=0}^{\infty}\{B_ne^{-i\nu_nL}+C_ne^{i\nu_nL}\}\int_{a}^{b}Y_m(y)Y_n(y)dy\\ &\quad-\frac{i}{\xi}\sum_{n=0}^{\infty}\{B_ne^{-i\nu_nL}+C_ne^{i\nu_nL}\}\int_{-b}^{-a}Y_m(y)Y_n(y)dy.\end{aligned}\tag{3.60}$$

On using (3.49) and (3.50) into (3.60), we get

$$\begin{aligned}B_me^{-i\nu_mL}-C_me^{i\nu_mL}&=\frac{R_{0m}}{E_m\nu_m}-\frac{1}{E_m\nu_m}\sum_{n=0}^{\infty}A_n\eta_nR_{nm}\\ &\quad-\frac{1}{E_m\nu_m\xi}\sum_{n=0}^{\infty}\{B_ne^{-i\nu_nL}+C_ne^{i\nu_nL}\}P_{mn}\\ &\quad-\frac{1}{E_m\nu_m\xi}\sum_{n=0}^{\infty}\{B_ne^{-i\nu_nL}+C_ne^{i\nu_nL}\}Q_{mn},\end{aligned}\tag{3.61}$$

where

$$P_{mn} = \int_a^b Y_n(y)Y_m(y)dy \tag{3.62}$$

and

$$Q_{mn} = \int_{-b}^{-a} Y_n(y)Y_m(y)dy. \tag{3.63}$$

By using (3.30) and (3.31) into the condition of normal velocity (3.58), we have

$$\begin{aligned} & i\sum_{n=0}^{\infty}\{B_n e^{i\nu_n L} - C_n e^{-i\nu_n L}\}\nu_n Y_n(y) = \\ & \begin{cases} \frac{i}{\xi}\sum_{n=0}^{\infty}\{B_n e^{i\nu_n L} + C_n e^{-i\nu_n L}\}Y_n(y), & a \leqslant y \leqslant b, \\ i\sum_{n=0}^{\infty} D_n\eta_n \cos\{\frac{n\pi}{2a}(y+a)\}, & -a \leqslant y \leqslant a, \\ \frac{i}{\xi}\sum_{n=0}^{\infty}\{B_n e^{i\nu_n L} + C_n e^{-i\nu_n L}\}Y_n(y), & -b \leqslant y \leqslant -a. \end{cases} \end{aligned} \tag{3.64}$$

By multiplying (3.62) by $Y_m(y)$ and then integrating with respect to y over $-b \leqslant y \leqslant b$, we obtain

$$\begin{aligned} & i\sum_{n=0}^{\infty}\{B_n e^{i\nu_n L} - C_n e^{-i\nu_n L}\}\nu_n \int_{-b}^{b} Y_m(y)Y_n(y)dy \\ & = \frac{i}{\xi}\sum_{n=0}^{\infty}\{B_n e^{i\nu_n L} + C_n e^{-i\nu_n L}\}\int_a^b Y_m(y)Y_n(y)dy \\ & \qquad + i\sum_{n=0}^{\infty} D_n\eta_n \int_{-a}^{a} Y_m(y)\cos\{\frac{n\pi}{2a}(y+a)\}dy \\ & + \frac{i}{\xi}\sum_{n=0}^{\infty}\{B_n e^{i\nu_n L} + C_n e^{-i\nu_n L}\}\int_{-b}^{-a} Y_m(y)Y_n(y)dy. \end{aligned} \tag{3.65}$$

Using (3.49) and (3.50) into (3.65), we have

$$\begin{aligned} B_m e^{i\nu_m L} - C_m e^{-i\nu_m L} &= \frac{1}{E_m\nu_m}\sum_{n=0}^{\infty} D_n\eta_n R_{nm} \\ & + \frac{1}{E_m\nu_m\xi}\sum_{n=0}^{\infty}\{B_n e^{i\nu_n L} + C_n e^{-i\nu_n L}\}P_{mn} \\ & + \frac{1}{E_m\nu_m\xi}\sum_{n=0}^{\infty}\{B_n e^{i\nu_n L} + C_n e^{-i\nu_n L}\}Q_{mn}. \end{aligned} \tag{3.66}$$

By adding (3.61) and (3.66), we found

$$L_m^- = \frac{R_{0m}}{2\cos(\nu_m L)E_m\nu_m} - \frac{1}{2\cos(\nu_m L)E_m\nu_m}\sum_{n=0}^{\infty}\Psi_n^-\eta_n R_{nm} + \frac{i}{\cos(\nu_m L)E_m\nu_m\xi}\sum_{n=0}^{\infty}L_n^-\sin(\nu_n L)P_{mn} + \frac{i}{\cos(\nu_m L)E_m\nu_m\xi}\sum_{n=0}^{\infty}L_n^-\sin(\nu_n L)Q_{mn}. \tag{3.67}$$

By subtracting (3.61) and (3.66), we obtain

$$L_m^+ = -\frac{R_{0m}}{2i\sin(\nu_m L)E_m\nu_m} + \frac{1}{2i\sin(\nu_m L)E_m\nu_m}\sum_{n=0}^{\infty}\Psi_n^+\eta_n R_{nm} + \frac{1}{\sin(\nu_m L)E_m\nu_m\xi}\sum_{n=0}^{\infty}L_n^+\cos(\nu_n L)P_{mn} + \frac{1}{\sin(\nu_m L)E_m\nu_m\xi}\sum_{n=0}^{\infty}L_n^+\cos(\nu_n L)Q_{mn}. \tag{3.68}$$

Similarly we find a system of equations defined by (3.43) and (3.68) with unknowns L_m^+ and Ψ_m^+. Also a system for unknowns L_m^- and Ψ_m^- is defined in (3.44) and (3.67). These systems are truncated and solved numerically for $L_m^\pm$ and $\Psi_m^\pm$. Then the model coefficients $\{A_m, B_m, C_m, D_m\}$ are achieved from these values $L_m^\pm$ and $\Psi_m^\pm$. In the next section we calculate the propagation and scattering energy flux.

3.3 Energy Flux

Here using equation (2.10) the incident energy flux P_{inc} in region R_1 is given by

$$P_{inc} = \frac{1}{2}Re\left[i\int_{-a}^{a}\phi_{inc}\left(\frac{\partial\phi_{inc}}{\partial n}\right)^{\star}dy\right]. \tag{3.69}$$

Using the incident field $\phi_{inc} = e^{i(x+L)}$ in the above equation, we have

$$P_{inc} = \frac{1}{2}Re\left[i\int_{-a}^{a}e^{i(x+L)}(-ie^{-i(x+L)})dy\right]. \tag{3.70}$$

$$P_{inc} = a. \tag{3.71}$$

Similarly the reflected energy P_{ref} in region R_1 is found by using reflected field potential $\phi_{ref}(x, y)$ into (2.10), that gives

$$P_{ref} = \frac{1}{2} Re \left[i \int_{-a}^{a} \phi_{ref} \left(\frac{\partial \phi_{ref}}{\partial n} \right)^{\star} dy \right]. \tag{3.72}$$

Using (3.22) into (3.72), we get

$$\begin{aligned} P_{ref} = \frac{1}{2} Re \big[- \sum_{n=0}^{\infty} \sum_{m=0}^{\infty} A_n A_m^{\star} \eta_m^{\star} e^{-i(x+L)(\eta_n - \eta_m^{\star})} \\ \int_{-a}^{a} \cos\left(\frac{m\pi}{2a}(y+a) \right) \cos\left(\frac{n\pi}{2a}(y+a) \right) dy \big]. \end{aligned} \tag{3.73}$$

Then by using the orthogonality relation (3.36) into (3.73), we obtain

$$P_{ref} = -\frac{a}{2} Re \left[\sum_{n=0}^{\infty} A_n A_n^{\star} \eta_n^{\star} e^{-i(x+L)(\eta_n - \eta_n^{\star})} \epsilon_n \right],$$

where the wave number η_n , $n = 0, 1, 2, ...$ is either real or imaginary, so for both cases, real part of (3.73) is given by

$$P_{ref} = -\frac{a}{2} Re \left[\sum_{n=0}^{\infty} \mid A_n \mid^2 \epsilon_n \eta_n \right]. \tag{3.74}$$

The negative sign here denotes that the reflected energy propagates in opposite direction to the incident energy. Similarly, the energy flux P_{tr} in region R_3 can be found by using transmitted field potential ϕ_{tr} in (3.31), we found

$$P_{tr} = \frac{a}{2} Re \left[\sum_{n=0}^{\infty} \mid D_n \mid^2 \epsilon_n \eta_n \right]. \tag{3.75}$$

Since energy is incident from region R_1 and transmitted from region R_3, then energy flux can be written as:

$$P_{inc} + P_{ref} = P_{tr}. \tag{3.76}$$

On using (3.71), (3.74) and (3.75) into (3.76), we get

$$a - \frac{a}{2} Re \left[\sum_{n=0}^{\infty} \mid A_n \mid^2 \epsilon_n \eta_n \right] = \frac{a}{2} Re \left[\sum_{n=0}^{\infty} \mid D_n \mid^2 \epsilon_n \eta_n \right]. \tag{3.77}$$

By dividing $\frac{2}{a}$ on both sides, we found the desired result as:

$$1 = \zeta_{ref} + \zeta_{tr}, \tag{3.78}$$

where

$$\zeta_{ref} = \frac{1}{2} Re \left[\sum_{n=0}^{\infty} \mid A_n \mid^2 \epsilon_n \eta_n \right] \tag{3.79}$$

and

$$\zeta_{tr} = \frac{1}{2} Re \left[\sum_{n=0}^{\infty} \mid D_n \mid^2 \epsilon_n \eta_n \right], \tag{3.80}$$

where the incident power being scaled at unity. By using equation (3.80) and incident energy flux that is unity, equation (2.11) yields the transmission loss as

$$TL = -10 \log_{10} (\zeta_{tr}). \tag{3.81}$$

3.4 Numerical Results and Discussion

Here the systems of equations achieved for rigid case (3.43)-(3.44) and (3.55)-(3.56), where for vertical lining (3.43)-(3.44) and (3.67)-(3.68) are truncated by $n = m = 0, 1, 2, \ldots, N$ terms. Then each system is solved separately for respected unknowns. In this way we get the model coefficients $\{A_n, B_n, C_n, D_n\}$, $n = 0, 1, 2..., N$ terms for rigid vertical case and vertical lining case separately. The truncated solutions are used to reconstruct the matching conditions at interfaces. For computation the speed of sound $c = 343.5 ms^{-1}$ and density of air $\rho = 1.2043 kgm^{-3}$ remain fixed.

For fibrous and perforated sheets the value of absorbing materials varies as:

fibrous sheet: $\xi = 0.5, \quad -1.0 < \eta < 3.0,$

perforated sheet: $0 < \xi < 3.0, \quad -1.0 < \eta < 3.0.$

Likewise dimensional duct heights, frequency and terms are fixed at $a^* = 0.08m$, $b^* = 0.28m$, $f = 250Hz$ and $N = 25$.

For rigid vertical case the pressure and velocity graphs are shown in Figures 3.7-3.10 and 3.3-3.6 respectively. It can be seen that the pressure and velocity curves coincide. It confirms the reconstruction of matching conditions at interfaces as assumed in equations (3.32)-(3.33) and (3.45)-(3.46).

Similarly for vertical absorbing lining case the pressure and velocity graphs are shown in Figures 3.15-3.18 and 3.11-3.14 respectively. It can be seen that the pressure and velocity curves coincide. It confirms the reconstruction of matching conditions at interfaces as assumed in equations (3.32)-(3.33) and (3.57)-(3.58).

Moreover, in Figures 3.19-3.22 the transmission loss is plotted against frequency to insight the problems physically. It is found that more transmission loss with fibrous case than perforated case is obtained.

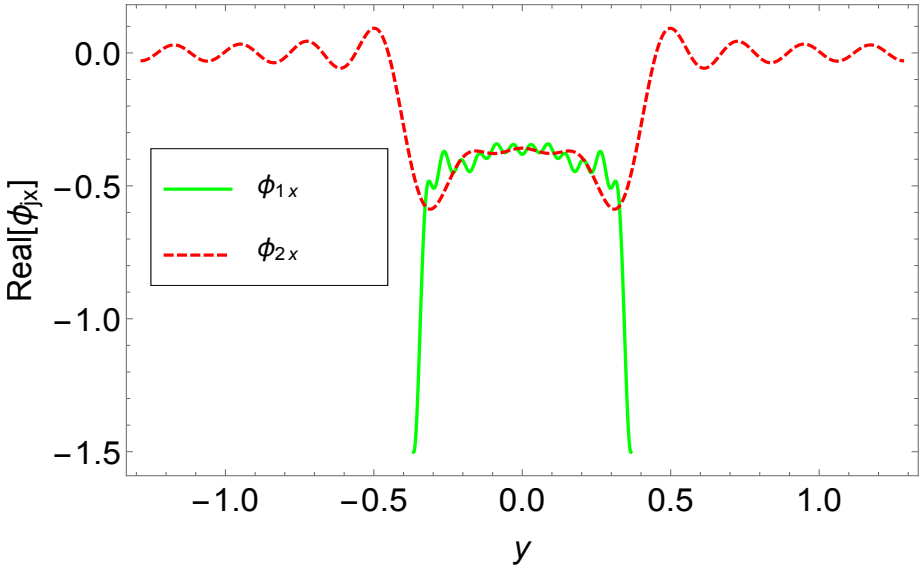

FIGURE 3.3: The real parts of velocities for rigid vertical strips at -L.

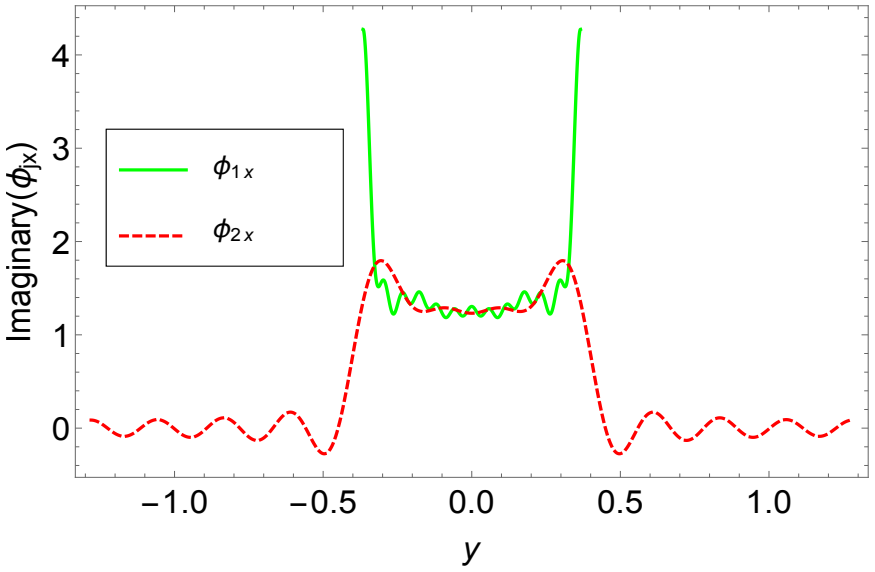

FIGURE 3.4: The imaginary parts of velocities for rigid vertical strips at -L.

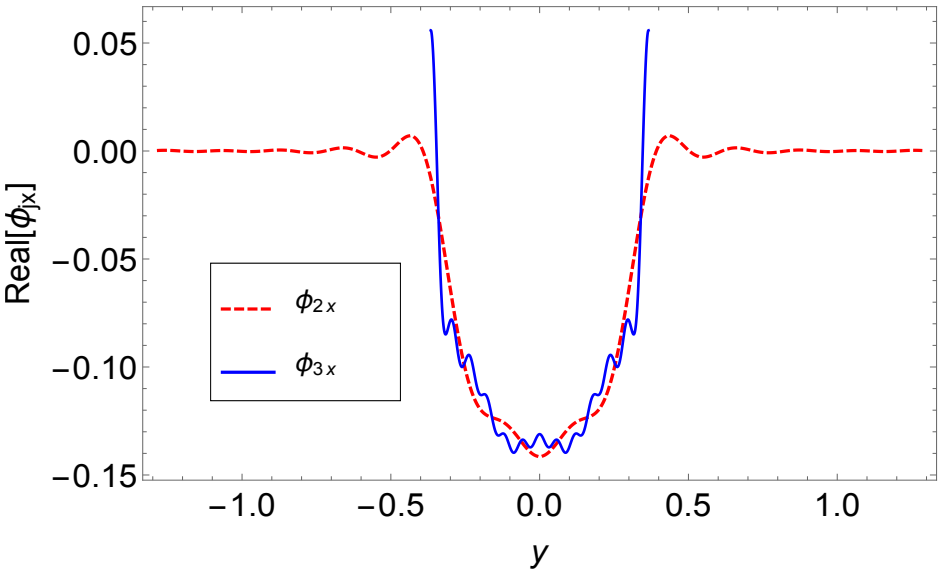

FIGURE 3.5: The real parts of velocities for rigid vertical strips at L.

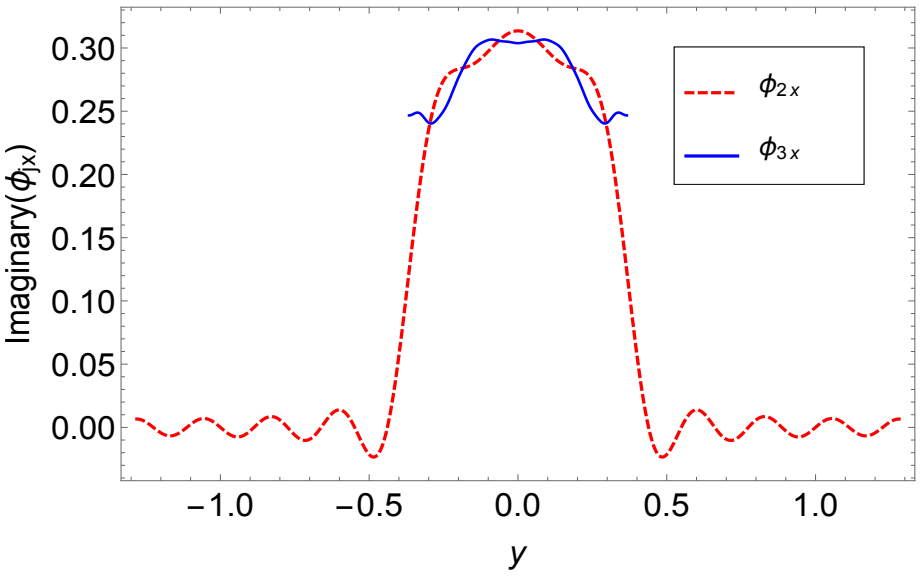

FIGURE 3.6: The imaginary parts of velocities for rigid vertical strips at L.

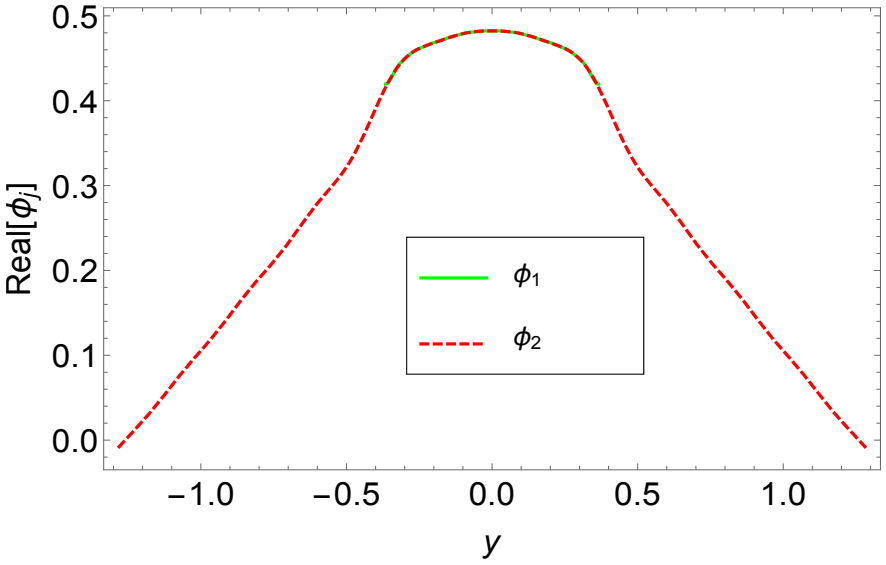

FIGURE 3.7: The real parts of pressures for rigid vertical strips at -L.

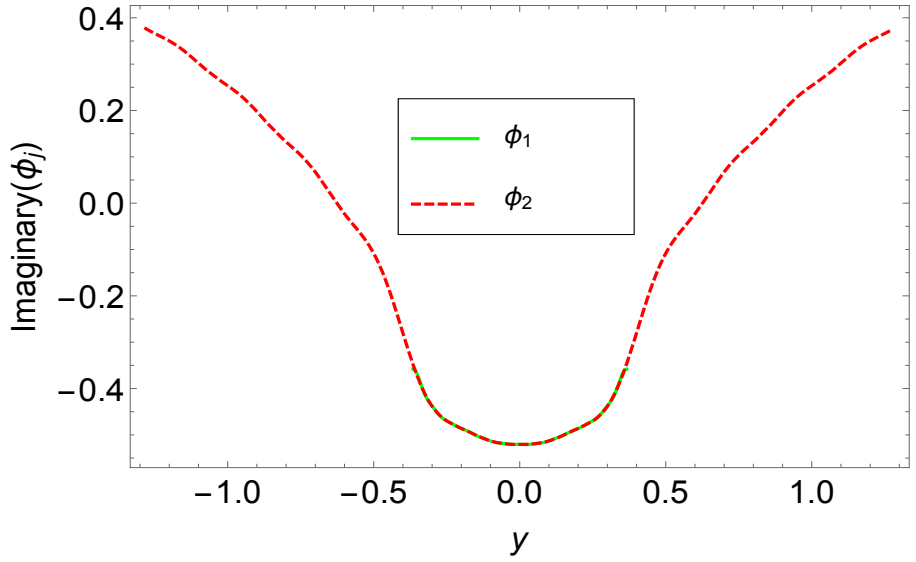

FIGURE 3.8: The imaginary parts of pressures for rigid vertical strips at -L.

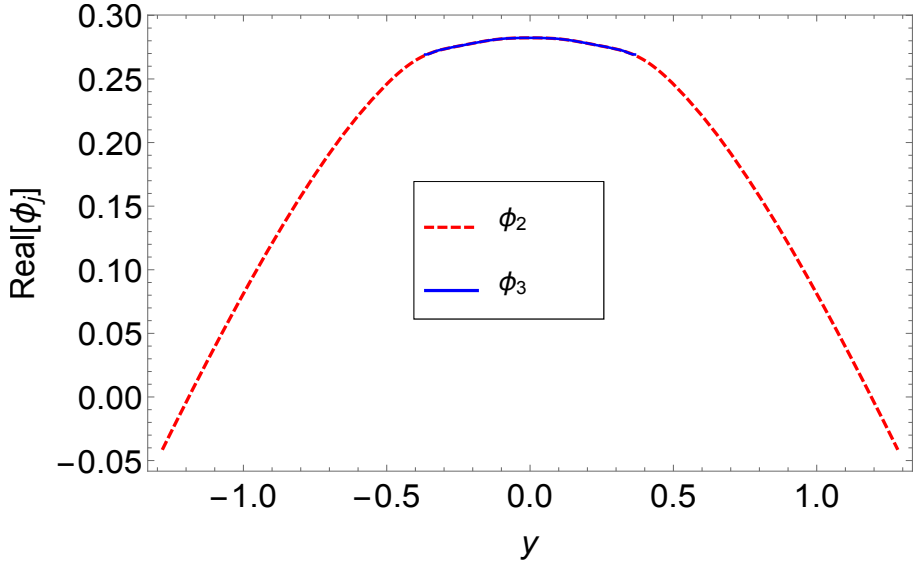

FIGURE 3.9: The real parts of pressures for rigid vertical strips at L.

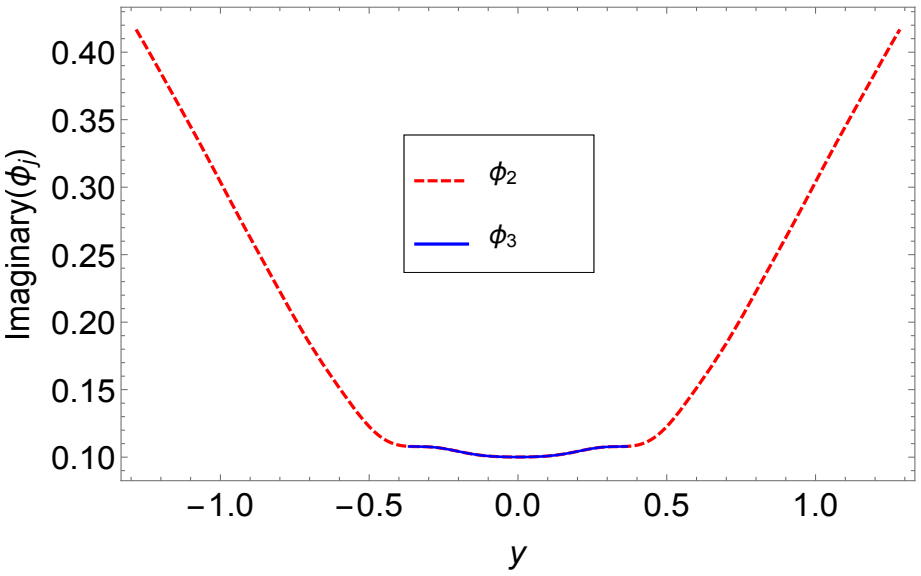

FIGURE 3.10: The imaginary parts of pressures for rigid vertical strips at L.

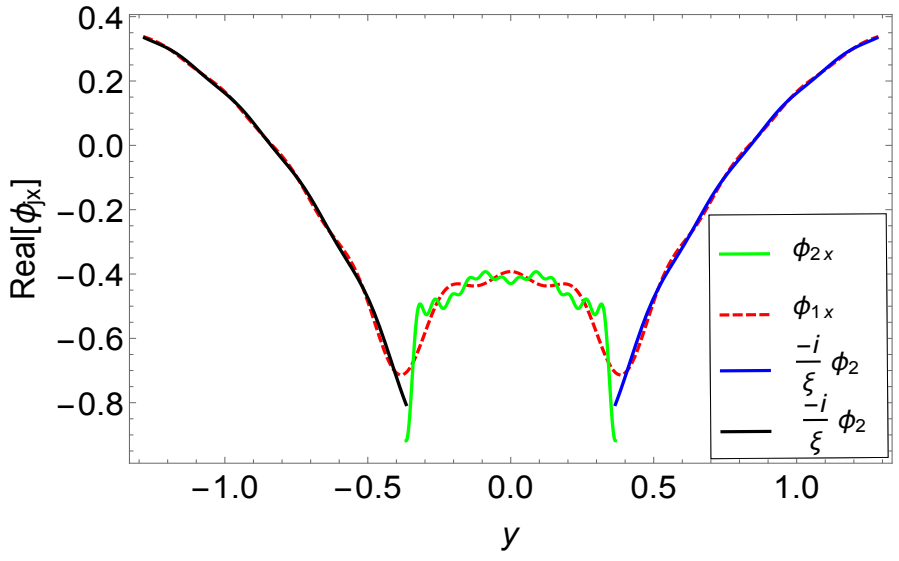

FIGURE 3.11: The real parts of velocities for vertical absorbing lining at -L.

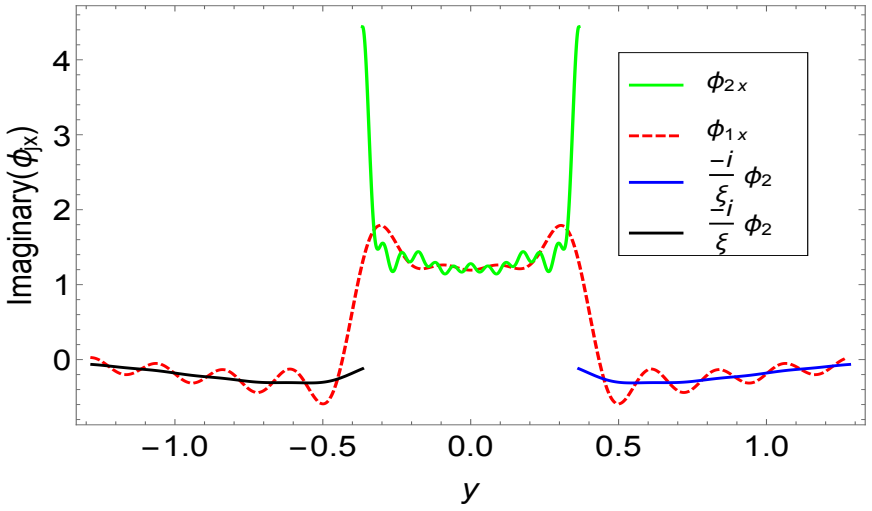

FIGURE 3.12: The imaginary parts of velocities for vertical absorbing lining at -L.

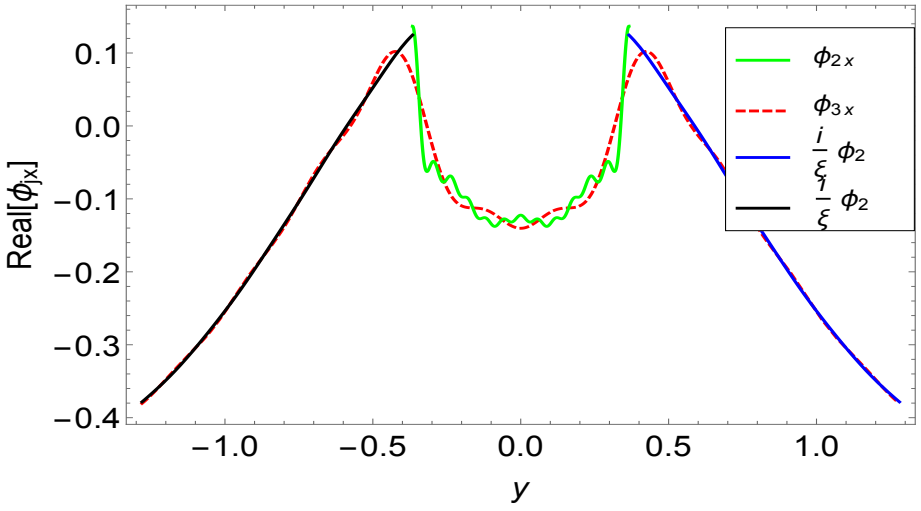

FIGURE 3.13: The real parts of velocities for vertical absorbing lining at L.

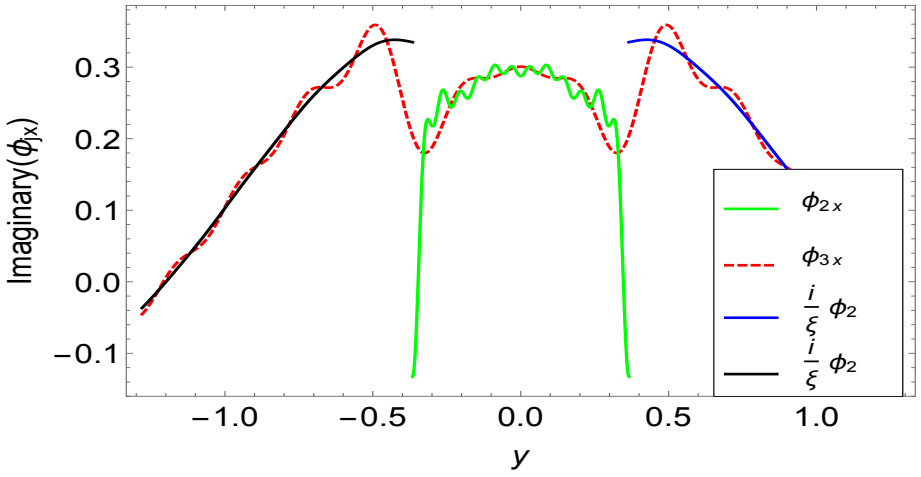

FIGURE 3.14: The imaginary parts of velocities for vertical absorbing lining at L.

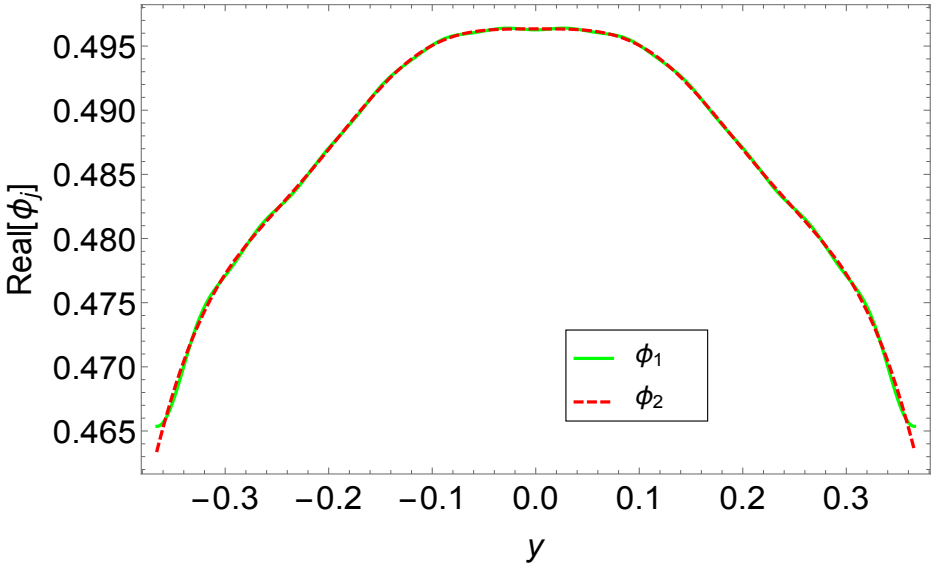

FIGURE 3.15: The real parts of pressures for vertical absorbing lining at -L.

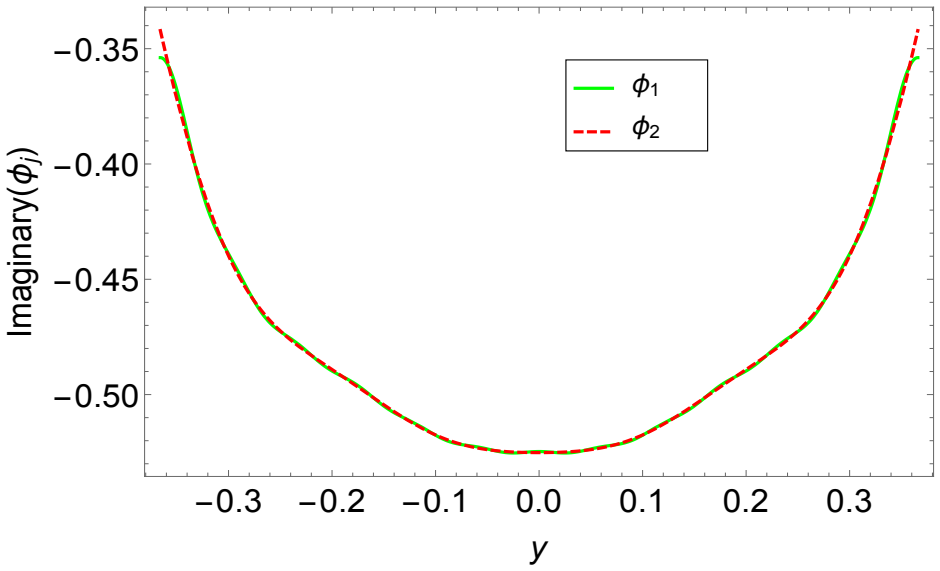

FIGURE 3.16: The imaginary parts of pressures for vertical absorbing lining at -L.

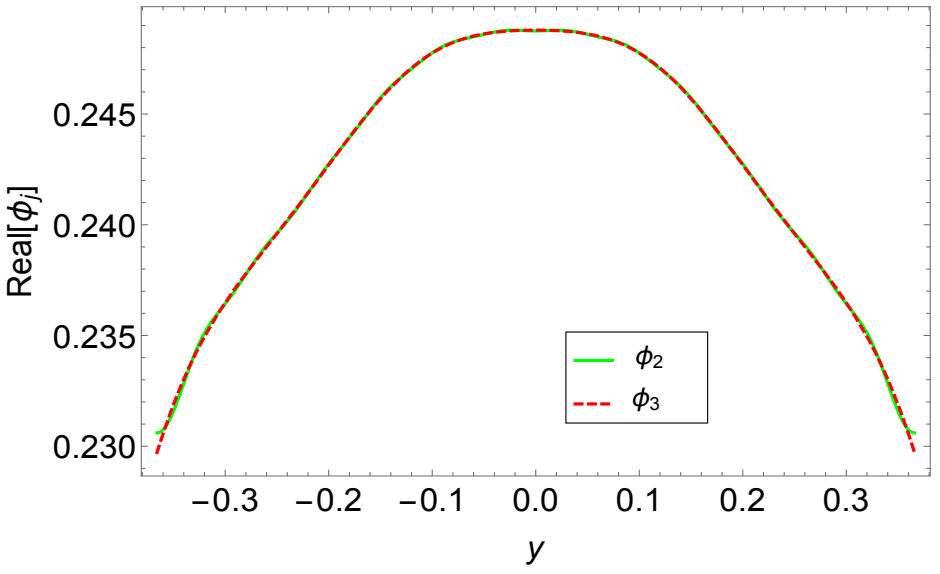

FIGURE 3.17: The real parts of pressures for vertical absorbing lining at L.

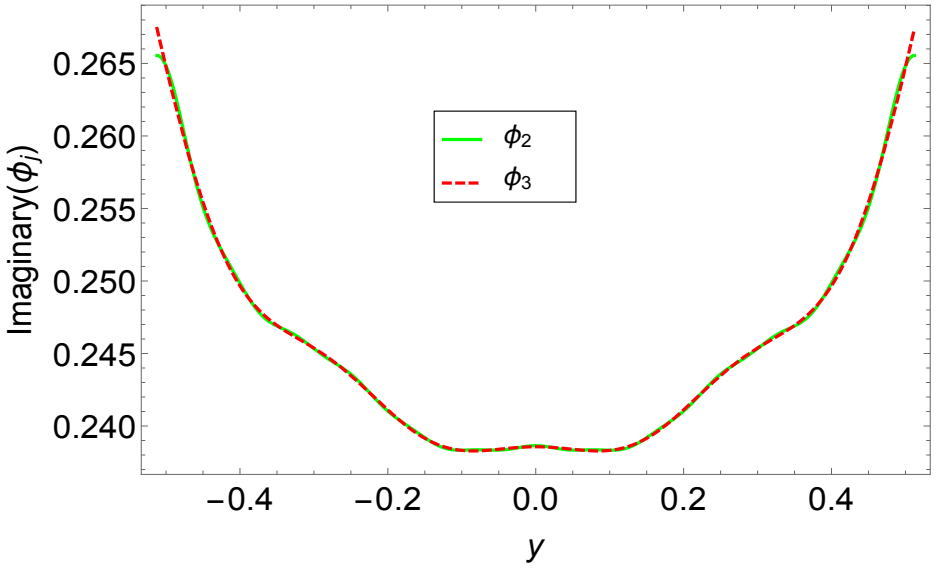

FIGURE 3.18: The imaginary parts of pressures for vertical absorbing lining at L.

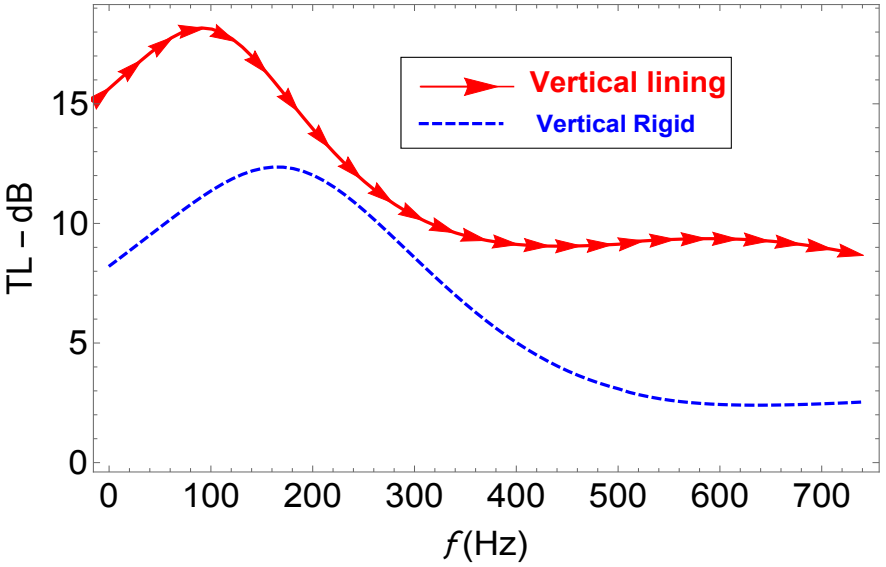

FIGURE 3.19: Transmission loss against frequency for rigid vertical and absorbing lining with $\xi = 0.5$ and $\eta = 0.5$.

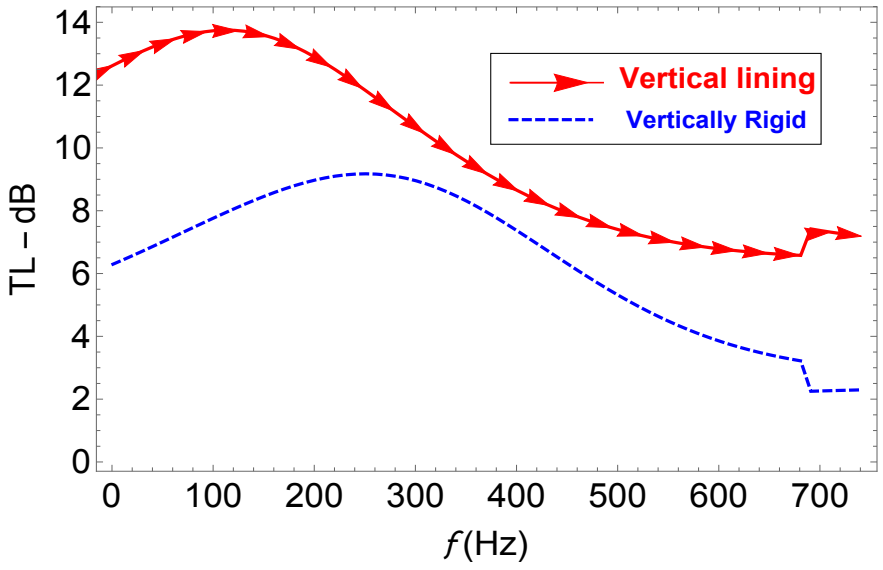

FIGURE 3.20: Transmission loss against frequency for rigid vertical and absorbing lining with $\xi = 1$ and $\eta = 0.5$.

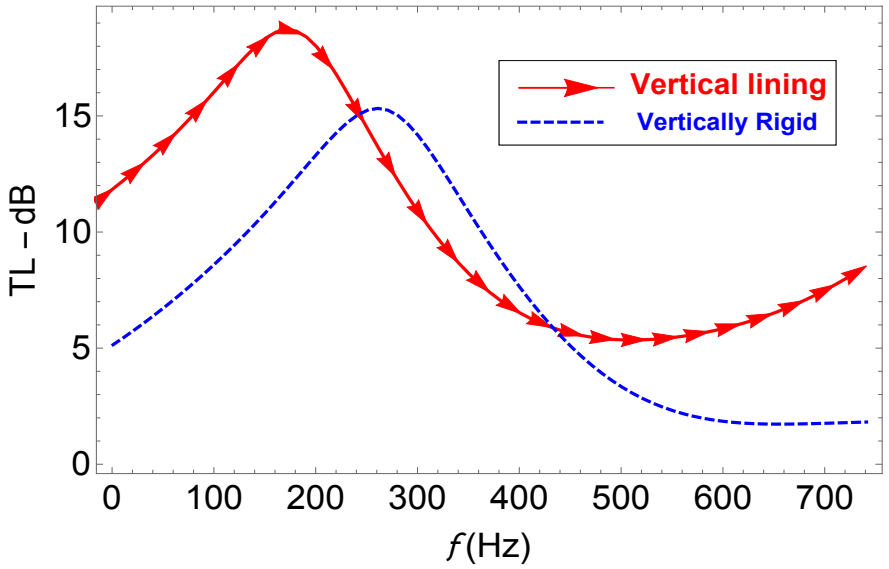

FIGURE 3.21: Transmission loss against frequency for rigid vertical and absorbing lining with $\xi = 0.5$ and $\eta = 1$.

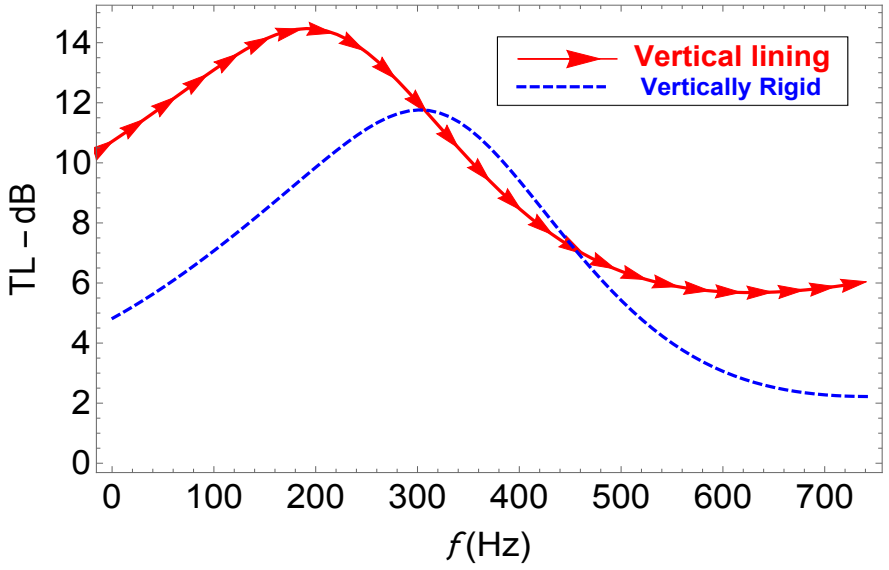

FIGURE 3.22: Transmission loss against frequency for rigid vertical and absorbing lining with $\xi = 1$ and $\eta = 1$.

Chapter 4

Scattering in Waveguide Involving Double Expansion Chambers

In this chapter we study the propagation and scattering of sound waves in acoustic waveguides involves double expansion chambers with absorbing lining. The governing boundary value problem is solved by using Mode Matching approach. The section wise detail discussed comprehensively in the following. In section 4.1 the mathematical formulation of the boundary value problem is given. In section 4.2 Mode Matching Solution of the boundary value problem are provided. In section 4.3 the derivation of energy flux is given. In section 4.4 the numerical results and discussion are given.

4.1 Mathematical Formulation

This section is extension of previous chapter (3), that involves double expansion chambers with absorbing lining. The horizontal boundaries of side regions at $y^* = \pm a^*$ are rigid whereas the boundaries of central region contain absorbing lining. The vertical boundaries at $x^* = \pm L^*$ and $x^* = \pm 2L^*$ can be of two different

categories:

1) Acoustical rigid.

2) Absorbing lining.

The geometrical configuration of the problem is shown in Figure 4.1. With refer-

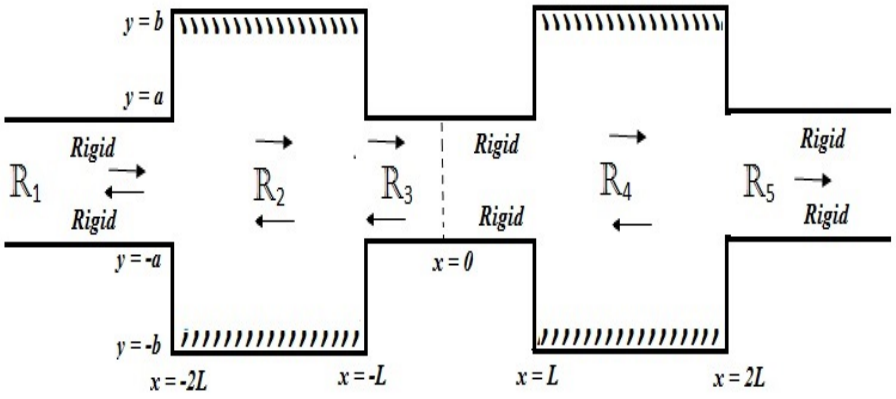

FIGURE 4.1: Geometry of the problem.

ence to different duct regions, this field potential can be written as:

$$\phi(x,y) = \begin{cases} \phi_1(x,y), & x < -2L, \quad |\, y \,| < a, \\ \phi_2(x,y), & |\, x \,| < -L, \quad y < b, \\ \phi_3(x,y), & x > -L, \quad |\, y \,| < a, \\ \phi_4(x,y), & |\, x \,| < L, \quad y < b, \\ \phi_5(x,y), & x > 2L, \quad |\, y \,| < a. \end{cases} \tag{4.1}$$

The dimensionless form of boundary conditions can be written as:

$$\frac{\partial \phi_1}{\partial y} = 0, \qquad x < -2L, \quad y = \pm a, \tag{4.2}$$

$$\phi_2 \pm i\xi \frac{\partial \phi_2}{\partial y} = 0, \quad |\, x \,| < -L, \quad y = \pm b, \tag{4.3}$$

$$\frac{\partial \phi_3}{\partial y} = 0, \qquad x < L, \quad y = \pm a, \tag{4.4}$$

$$\phi_4 \pm i\xi \frac{\partial \phi_4}{\partial y} = 0, \quad |\, x \,| < 2L, \quad y = \pm b, \tag{4.5}$$

$$\frac{\partial \phi_5}{\partial y} = 0, \qquad x > 2L, \quad y = \pm a. \tag{4.6}$$

The boundaries along the vertical strips can be rigid or absorbing lining. The rigid vertical boundaries (shown in Figure 4.1) are

$$\frac{\partial \phi_2}{\partial x} = 0, \quad y = -2L, \quad a \leqslant x \leqslant b, \qquad \frac{\partial \phi_2}{\partial x} = 0, \quad y = -L, \quad a \leqslant x \leqslant b \tag{4.7}$$

and

$$\frac{\partial \phi_4}{\partial x} = 0, \quad y = L, \quad a \leqslant x \leqslant b, \qquad \frac{\partial \phi_4}{\partial x} = 0, \quad y = 2L, \quad a \leqslant x \leqslant b. \tag{4.8}$$

The vertical absorbing lining boundaries (shown in Figure 4.2) are given by,

$$\phi_2 - i\xi \frac{\partial \phi_2}{\partial x} = 0, \; y = -2L, \quad a \leqslant x \leqslant b, \quad \phi_2 + i\xi \frac{\partial \phi_2}{\partial x} = 0, \; y = -L, \quad a \leqslant x \leqslant b \tag{4.9}$$

and

$$\phi_4 - i\xi \frac{\partial \phi_4}{\partial x} = 0, \; y = L, \quad a \leqslant x \leqslant b, \quad \phi_4 + i\xi \frac{\partial \phi_4}{\partial x} = 0, \; y = 2L, \quad a \leqslant x \leqslant b. \tag{4.10}$$

Now the boundary value problem is solved by using Mode-Matching technique.

4.2 Mode Matching Solution

Here we find the Mode Matching solution of the boundary value problem formulated in section 4.1. Consider a plane wave incident ϕ_{inc} which is fundamental duct mode of region $x < -2L$ is propagating from negative x-direction towards $|\, x \,| \leqslant 2L$, where it will scatter into the infinite number of reflected and transmitted modes.

The eigenfunction expansions forms for all duct regions are defined as:

$$\phi_1(x,y) = e^{i(x+2L)} + \sum_{n=0}^{\infty} A_n \cos\{\frac{n\pi}{2a}(y+a)\}e^{-i\eta_n(x+2L)}, \tag{4.11}$$

$$\phi_2(x,y) = \sum_{n=0}^{\infty}\{B_n e^{i\nu_n(x+L)} + C_n e^{-i\nu_n(x+L)}\}Y_n(y), \tag{4.12}$$

$$\phi_3(x,y) = \sum_{n=0}^{\infty}\{D_n e^{i\eta_n x} + E_n e^{-i\eta_n x}\}\cos\{\frac{n\pi}{2a}(y+a)\}, \tag{4.13}$$

$$\phi_4(x,y) = \sum_{n=0}^{\infty}\{F_n e^{i\nu_n(x-L)} + G_n e^{-i\nu_n(x-L)}\}Y_n(y), \tag{4.14}$$

and

$$\phi_5(x,y) = \sum_{n=0}^{\infty} H_n \cos\{\frac{n\pi}{2a}(y+a)\}e^{+i\eta_n(x-2L)}, \tag{4.15}$$

where $\eta_n = \sqrt{1-\tau_n^2}$, $n = 0, 1, 2, \ldots$ are the wave number of propagating modes in regions R_1, R_3 and R_5, where $\tau_n = n\pi/2a$, $n = 0, 1, 2, \ldots$. Also $\nu_n = \sqrt{1-\gamma_n^2}$ is the wave number of the propagating n^{th} mode. On using (4.3) and (4.5) into (3.27), we get the eigenfunctions in R_2 and R_4 as:

$$Y_n(y) = \sin\gamma_n(y+b) + i\xi_n\gamma_n\cos\gamma_n(y+b), \tag{4.16}$$

where γ_n, $n = 0, 1, 2, \ldots$ the eigen values are the roots of characteristic equation:

$$\sin\gamma_n(2b) + 2i\xi_n\gamma_n\cos(2\gamma_n b) + \xi_n^2\gamma_n^2\sin(2\gamma_n b) = 0. \tag{4.17}$$

These roots can be obtained numerically. Here the coefficient $\{A_n, C_n, E_n, G_n\}$, $n = 0, 1, 2, \ldots$ are the amplitudes of n^{th} reflected duct modes and the coefficient $\{B_n, D_n, F_n, H_n\}$, $n = 0, 1, 2, \ldots$ are the amplitudes of n^{th} transmitted duct modes. Note that these modal coefficients are unknowns. To determine these unknowns we use the matching procedure.

First we match the pressures across the regions at interfaces $x = \pm L$, $x = \pm 2L$. The continuity conditions of pressures are defined by

$$\phi_1(-2L, y) = \phi_2(-2L, y), \quad -a \leqslant y \leqslant a, \tag{4.18}$$

$$\phi_3(-L, y) = \phi_2(-L, y), \qquad -a \leqslant y \leqslant a, \tag{4.19}$$

$$\phi_3(L, y) = \phi_4(L, y), \qquad -a \leqslant y \leqslant a \tag{4.20}$$

and

$$\phi_5(2L, y) = \phi_4(2L, y), \qquad -a \leqslant y \leqslant a. \tag{4.21}$$

On using (4.11) and (4.12) into continuity condition of pressure (4.18), we found

$$1 + \sum_{n=0}^{\infty} A_n \cos\{\frac{n\pi}{2a}(y+a)\} = \sum_{n=0}^{\infty} \{B_n e^{-i\nu_n L} + C_n e^{i\nu_n L}\} Y_n(y). \tag{4.22}$$

On multiplying (4.22) with $\cos\{\frac{m\pi}{2a}(y+a)\}$ and integrating with respect to y over $-a \leqslant y \leqslant a$, we obtain

$$\begin{aligned} &\int_{-a}^{a} \cos\{\frac{m\pi}{2a}(y+a)\} dy + \sum_{n=0}^{\infty} A_n \int_{-a}^{a} \cos\{\frac{m\pi}{2a}(y+a)\} \cos\{\frac{n\pi}{2a}(y+a)\} dy \\ &= \sum_{n=0}^{\infty} \{B_n e^{-i\nu_n L} + C_n e^{i\nu_n L}\} \int_{-a}^{a} \cos\{\frac{m\pi}{2a}(y+a)\} Y_n(y) dy. \end{aligned} \tag{4.23}$$

On using (3.36) and (3.37) into (4.23), we get

$$A_m = -\delta_{m0} + \frac{1}{\epsilon_m a} \sum_{n=0}^{\infty} \{B_n e^{-i\nu_n L} + C_n e^{i\nu_n L}\} R_{mn}. \tag{4.24}$$

By using (4.12) and (4.13) into continuity condition of pressure (4.19), we obtain

$$\sum_{n=0}^{\infty} \{D_n e^{-i\eta_n L} + E_n e^{i\eta_n L}\} \cos\{\frac{n\pi}{2a}(y+a)\} = \sum_{n=0}^{\infty} \{B_n + C_n\} Y_n(y). \tag{4.25}$$

On multiplying (4.25) with $\cos\{\frac{m\pi}{2a}(y+a)\}$ and integrating with respect to y over $-a \leqslant y \leqslant a$, we have

$$\begin{aligned} &\sum_{n=0}^{\infty} \{D_n e^{-i\eta_n L} + E_n e^{i\eta_n L}\} \int_{-a}^{a} \cos\{\frac{m\pi}{2a}(y+a)\} \cos\{\frac{n\pi}{2a}(y+a)\} dy \\ &= \sum_{n=0}^{\infty} \{B_n + C_n\} \int_{-a}^{a} \cos\{\frac{m\pi}{2a}(y+a)\} Y_n(y) dy. \end{aligned} \tag{4.26}$$

Using (3.36) and (3.37) into (4.26), we found

$$D_m e^{-i\eta_m L} + E_m e^{i\eta_m L} = \frac{1}{a\epsilon_m} \sum_{n=0}^{\infty} \{B_n + C_n\} R_{mn}. \tag{4.27}$$

By using (4.13) and (4.14) into continuity condition of pressure (4.20), we get

$$\sum_{n=0}^{\infty} \{D_n e^{i\eta_n L} + E_n e^{-i\eta_n L}\} \cos\{\frac{n\pi}{2a}(y+a)\} = \sum_{n=0}^{\infty} \{F_n + G_n\} Y_n(y). \tag{4.28}$$

On multiplying (4.28) with $\cos\{\frac{m\pi}{2a}(y+a)\}$ and integrating with respect to y over $-a \leqslant y \leqslant a$, we found

$$\begin{aligned} &\sum_{n=0}^{\infty} \{D_n e^{i\eta_n L} + E_n e^{-i\eta_n L}\} \int_{-a}^{a} \cos\{\frac{m\pi}{2a}(y+a)\} \cos\{\frac{n\pi}{2a}(y+a)\} dy \\ &= \sum_{n=0}^{\infty} \{F_n + G_n\} \int_{-a}^{a} \cos\{\frac{m\pi}{2a}(y+a)\} Y_n(y) dy. \end{aligned} \tag{4.29}$$

Using (3.36) and (3.37) into (4.29), we found that

$$D_m e^{i\eta_m L} + E_m e^{-i\eta_m L} = \frac{1}{a\epsilon_m} \sum_{n=0}^{\infty} \{F_n + G_n\} R_{mn}. \tag{4.30}$$

Also using (4.14) and (4.15) into continuity condition of pressure (4.21), we obtain

$$\sum_{n=0}^{\infty} H_n \cos\{\frac{n\pi}{2a}(y+a)\} = \sum_{n=0}^{\infty} \{F_n e^{i\nu_n L} + G_n e^{-i\nu_n L}\} Y_n(y). \tag{4.31}$$

By multiplying (4.31) with $\cos\{\frac{m\pi}{2a}(y+a)\}$ and integrating with respect to y over $-a \leqslant y \leqslant a$, we have

$$\begin{aligned} &\sum_{n=0}^{\infty} H_n \int_{-a}^{a} \cos\{\frac{m\pi}{2a}(y+a)\} \cos\{\frac{n\pi}{2a}(y+a)\} dy = \\ &\sum_{n=0}^{\infty} \{F_n e^{i\nu_n L} + G_n e^{-i\nu_n L}\} \int_{-a}^{a} \cos\{\frac{m\pi}{2a}(y+a)\} Y_n(y) dy. \end{aligned} \tag{4.32}$$

Using (3.36) and (3.37) into (4.32), we found

$$H_m = \frac{1}{\epsilon_m a}\sum_{n=0}^{\infty}\{F_n e^{i\nu_n L} + G_n e^{-i\nu_n L}\}R_{mn}. \tag{4.33}$$

By adding (4.24) and (4.33), it is found that

$$U_m^+ = -\delta_{m0} + \frac{1}{\epsilon_m a}\sum_{n=0}^{\infty}\{V_n^+ e^{-i\nu_n L} + W_n^+ e^{i\nu_n L}\}R_{mn} \tag{4.34}$$

And subtracting (4.24) and (4.33), we obtain,

$$U_m^- = -\delta_{m0} + \frac{1}{\epsilon_m a}\sum_{n=0}^{\infty}\{V_n^- e^{-i\nu_n L} - W_n^- e^{i\nu_n L}\}R_{mn}, \tag{4.35}$$

where $U_m^{\pm} = (A_m \pm H_m)$ and $V_n^{\pm} = (B_n \pm G_n)$ and $W_n^{\pm} = (F_n \pm C_n)$. Likewise adding (4.27) and (4.30), we have

$$Z_m^+ = \frac{1}{2a\cos(\eta_m L)\epsilon_m}\sum_{n=0}^{\infty}\{V_n^+ + W_n^+\}R_{mn}. \tag{4.36}$$

Similarly subtracting (4.27) and (4.30), we get

$$Z_m^- = \frac{-1}{2ai\sin(\eta_m L)\epsilon_m}\sum_{n=0}^{\infty}\{V_n^- - W_n^-\}R_{mn}, \tag{4.37}$$

where $Z_m^{\pm} = (D_m \pm E_m)$ and $Z_n^{\pm} = (D_n \pm E_n)$. Now we apply the continuity conditions of normal velocities. Two cases are considered herein depending upon the properties of vertical strips, that are

1) Rigid vertical strips.

2) Porous linings along the vertical strips.

4.2.1 Rigid Vertical Strips

For this case the continuity conditions of normal velocities are defined by,

$$\phi_{2x}\left(-2L,y\right)=\begin{cases}0, & -b\leqslant y\leqslant -a,\\ \phi_{1x}\left(-2L,y\right), & -a\leqslant y\leqslant a,\\ 0, & a\leqslant y\leqslant b,\end{cases} \tag{4.38}$$

$$\phi_{2x}\left(-L,y\right)=\begin{cases}0, & -b\leqslant y\leqslant -a,\\ \phi_{3x}\left(-L,y\right), & -a\leqslant y\leqslant a,\\ 0, & a\leqslant y\leqslant b,\end{cases} \tag{4.39}$$

$$\phi_{4x}\left(L,y\right)=\begin{cases}0, & -b\leqslant y\leqslant -a,\\ \phi_{3x}\left(L,y\right), & -a\leqslant y\leqslant a,\\ 0, & a\leqslant y\leqslant b\end{cases} \tag{4.40}$$

and

$$\phi_{4x}\left(2L,y\right)=\begin{cases}0, & -b\leqslant y\leqslant -a,\\ \phi_{5x}\left(2L,y\right), & -a\leqslant y\leqslant a,\\ 0, & a\leqslant y\leqslant b.\end{cases} \tag{4.41}$$

On using (4.11) and (4.12) into the condition of normal velocity (4.38), we found that

$$i\sum_{n=0}^{\infty}\{B_ne^{-i\nu_nL}-C_ne^{i\nu_nL}\}\nu_nY_n(y)=$$
$$\begin{cases}0, & -b\leqslant y\leqslant -a,\\ i-i\sum_{n=0}^{\infty}A_n\eta_n\cos\{\frac{n\pi}{2a}(y+a)\}, & -a\leqslant y\leqslant a,\\ 0, & a\leqslant y\leqslant b.\end{cases} \tag{4.42}$$

We multiply (4.42) by $Y_m(y)$ and integrate with respect to y over $-b \leqslant y \leqslant b$, we obtain

$$i\sum_{n=0}^{\infty}\{B_n e^{-i\nu_n L} - C_n e^{i\nu_n L}\}\nu_n \int_{-b}^{b} Y_m(y)Y_n(y)dy =$$
$$i\int_{-a}^{a} Y_m(y)dy - i\sum_{n=0}^{\infty} A_n\eta_n \int_{-a}^{a} \cos\{\frac{n\pi}{2a}(y+a)\}Y_m(y)dy. \tag{4.43}$$

Using (3.49) and (3.50) into (4.43), we have

$$B_m e^{-i\nu_m L} - C_m e^{i\nu_m L} = \frac{R_{0m}}{E_m\nu_m} - \frac{1}{E_m\nu_m}\sum_{n=0}^{\infty} A_n\eta_n R_{nm}. \tag{4.44}$$

By using (4.12) and (4.13) into condition of normal velocity (4.39), we found

$$i\sum_{n=0}^{\infty}\{B_n - C_n\}\nu_n Y_n(y) = i\sum_{n=0}^{\infty}\{D_n e^{-i\eta_n L} - E_n e^{i\eta_n L}\}\eta_n \cos\{\frac{n\pi}{2a}(y+a)\}. \tag{4.45}$$

On multiplying (4.45) by $Y_m(y)$ and integrating with respect to y over $-b \leqslant y \leqslant b$, we obtain

$$i\sum_{n=0}^{\infty}\{B_n - C_n\}\int_{-b}^{b} Y_n(y)Y_m(y)dy =$$
$$i\sum_{n=0}^{\infty}\{D_n e^{-i\eta_n L} - E_n e^{i\eta_n L}\}\eta_n \int_{-a}^{a} Y_m(y)\cos\{\frac{n\pi}{2a}(y+a)\}Y_m(y)dy. \tag{4.46}$$

Using (3.49) and (3.50) into (4.46), we found that

$$B_m - C_m = \frac{1}{E_m\nu_m}\sum_{n=0}^{\infty}\{D_n e^{-i\eta_n L} - E_n e^{i\eta_n L}\}\eta_n R_{nm}. \tag{4.47}$$

On using (4.13) and (4.14) into condition of normal velocity (4.40), we obtain

$$i\sum_{n=0}^{\infty}\{F_n - G_n\}\nu_n Y_n(y) = i\sum_{n=0}^{\infty}\{D_n e^{i\eta_n L} - E_n e^{-i\eta_n L}\}\eta_n \cos\{\frac{n\pi}{2a}(y+a)\}. \tag{4.48}$$

We multiply (4.48) by $Y_m(y)$ and integrate with respect to y over $-b \leqslant y \leqslant b$, we have

$$i\sum_{n=0}^{\infty}\{F_n - G_n\}\int_{-b}^{b} Y_n(y)Y_m(y)dy =$$
$$i\sum_{n=0}^{\infty}\{D_n e^{i\eta_n L} - E_n e^{-i\eta_n L}\}\eta_n \int_{-a}^{a}\cos\{\frac{n\pi}{2a}(y+a)\}Y_m(y)dy. \tag{4.49}$$

Using (3.49) and (3.50) into (4.49), we get

$$F_m - G_m = \frac{1}{E_m\nu_m}\sum_{n=0}^{\infty}\{D_n e^{i\eta_n L} - E_n e^{-i\eta_n L}\}\eta_n R_{nm}. \tag{4.50}$$

On using (4.14) and (4.15) into condition of normal velocity (4.41), we obtain

$$i\sum_{n=0}^{\infty}\{F_n e^{i\nu_n L} - G_n e^{-i\nu_n L}\}\nu_n Y_n(y) = i\sum_{n=0}^{\infty} H_n\eta_n\cos\{\frac{n\pi}{2a}(y+a)\}. \tag{4.51}$$

By multiplying (4.51) by $Y_m(y)$ and integrating with respect to y over $-b \leqslant y \leqslant b$, we found

$$i\sum_{n=0}^{\infty}\{F_n e^{i\nu_n L} - G_n e^{-i\nu_n L}\}\int_{-b}^{b} Y_n(y)Y_m(y)dy =$$
$$i\sum_{n=0}^{\infty} H_n\eta_n\int_{-a}^{a}\cos\{\frac{n\pi}{2a}(y+a)\}Y_m(y)dy. \tag{4.52}$$

On using (3.49) and (3.50) into (4.52), we have

$$F_m e^{i\nu_m L} - G_m e^{-i\nu_m L} = \frac{1}{E_m\nu_m}\sum_{n=0}^{\infty} H_n\eta_n R_{nm}. \tag{4.53}$$

By subtracting (4.44) and (4.53), we obtain

$$V_m^+ e^{-i\nu_m L} - W_m^+ e^{i\nu_m L} = \frac{R_{0m}}{E_m\nu_m} - \frac{1}{E_m\nu_m}\sum_{n=0}^{\infty} U_n^+\eta_n R_{nm}. \tag{4.54}$$

On adding (4.44) and (4.53), we have

$$V_m^- e^{-i\nu_m L} + W_m^- e^{i\nu_m L} = \frac{R_{0m}}{E_m \nu_m} - \frac{1}{E_m \nu_m} \sum_{n=0}^{\infty} U_n^- \eta_n R_{nm}. \tag{4.55}$$

Similarly subtracting (4.47) and (4.50), we found

$$V_m^+ - W_m^+ = \frac{-2i}{E_m \nu_m} \sum_{n=0}^{\infty} Z_n^+ \sin(\eta_n L) \eta_n R_{nm}. \tag{4.56}$$

By adding (4.47) and (4.50), we get

$$V_m^- + W_m^- = \frac{2}{E_m \nu_m} \sum_{n=0}^{\infty} Z_n^- \cos(\eta_n L) \eta_n R_{nm}. \tag{4.57}$$

Thus we get a system of equations defined by (4.34) and (4.36), (4.54) and (4.56) with unknowns U_m^+, Z_m^+, V_m^+ and W_m^+. Also a system for unknowns U_m^-, Z_m^-, V_m^- and W_m^- is given in (4.35) and (4.37), (4.55) and (4.57). These systems are truncated and solved numerically for $U_m^{\pm}$, $Z_m^{\pm}$, $V_m^{\pm}$ and $W_m^{\pm}$. Then the model coefficients $\{A_m, B_m, C_m, D_m, E_m, F_m, G_m, H_m\}$ are found from these values $U_m^{\pm}$, $Z_m^{\pm}$, $V_m^{\pm}$ and $W_m^{\pm}$ as:

$$A_m = \frac{U_m^+ + U_m^-}{2}, \quad H_m = \frac{U_m^+ - U_m^-}{2},$$
$$B_m = \frac{V_m^+ + V_m^-}{2}, \quad G_m = \frac{V_m^+ - V_m^-}{2},$$
$$F_m = \frac{W_m^+ + W_m^-}{2}, \quad C_m = \frac{W_m^+ - W_m^-}{2},$$

and

$$D_m = \frac{Z_m^+ + Z_m^-}{2}, \quad E_m = \frac{Z_m^+ - Z_m^-}{2}.$$

4.2.2 Porous Linings along the Vertical Strips

In this subsection we study the propagation and scattering of acoustic waves in an acoustic waveguide which inserted double expansion chambers including absorbing lining. The geometrical configuration of the problem is shown in Figure 4.2. The present problem involving vertical absorbing lining in expansion chambers just effect the normal velocities of the waveguide. Here, we defined normal velocities

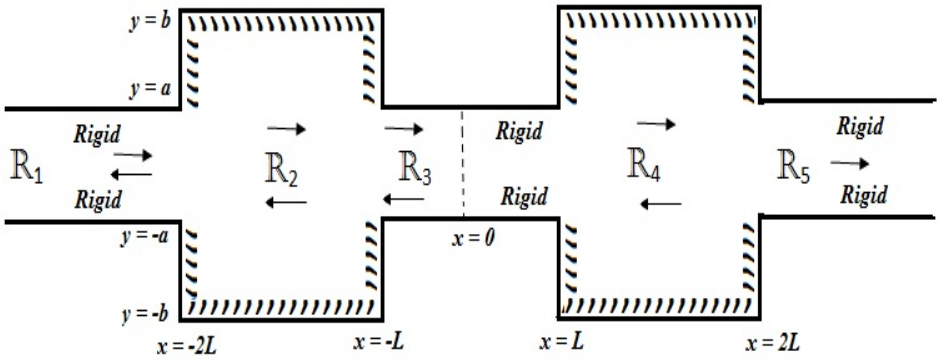

FIGURE 4.2: Geometry of the problem.

at $x = \pm L$ and $x = \pm 2L$.

The continuity conditions of normal velocities for this case are defined by,

$$\phi_{2x}(-2L, y) = \begin{cases} \phi_{1x}(-2L, y), & -a \leqslant y \leqslant a, \\ \dfrac{-i}{\xi}\phi_2(-2L, y), & a \leqslant y \leqslant b, \\ \dfrac{-i}{\xi}\phi_2(-2L, y), & -b \leqslant y \leqslant -a \end{cases} \tag{4.58}$$

$$\phi_{2x}(-L, y) = \begin{cases} \dfrac{i}{\xi}\phi_2(-L, y), & a \leqslant y \leqslant b, \\ \phi_{3x}(-L, y), & -a \leqslant y \leqslant a, \\ \dfrac{i}{\xi}\phi_2(-L, y), & -b \leqslant y \leqslant -a, \end{cases} \tag{4.59}$$

$$\phi_{4x}(L, y) = \begin{cases} \phi_{3x}(L, y), & -a \leqslant y \leqslant a, \\ \dfrac{-i}{\xi}\phi_4(L, y), & a \leqslant y \leqslant b, \\ \dfrac{-i}{\xi}\phi_4(L, y), & -b \leqslant y \leqslant -a \end{cases} \tag{4.60}$$

and

$$\phi_{4x}(2L,y)=\begin{cases}\dfrac{i}{\xi}\phi_4(2L,y), & a\leqslant y\leqslant b,\\ \phi_{5x}(2L,y), & -a\leqslant y\leqslant a,\\ \dfrac{i}{\xi}\phi_4(2L,y), & -b\leqslant y\leqslant -a.\end{cases}\tag{4.61}$$

On using (4.11) and (4.12) into the condition of normal velocity (4.58), we obtain

$$\begin{aligned}&i\sum_{n=0}^{\infty}\{B_ne^{-i\nu_nL}-C_ne^{i\nu_nL}\}\nu_nY_n(y)=\\ &\begin{cases}i-i\sum_{n=0}^{\infty}A_n\eta_n\cos\{\dfrac{n\pi}{2a}(y+a)\}, & -a\leqslant y\leqslant a,\\ \dfrac{-i}{\xi}\sum_{n=0}^{\infty}\{B_ne^{-i\nu_nL}+C_ne^{i\nu_nL}\}Y_n(y), & a\leqslant y\leqslant b,\\ \dfrac{-i}{\xi}\sum_{n=0}^{\infty}\{B_ne^{-i\nu_nL}+C_ne^{i\nu_nL}\}Y_n(y), & -b\leqslant y\leqslant -a.\end{cases}\end{aligned}\tag{4.62}$$

We multiply (4.62) by $Y_m(y)$ and integrate with respect to y over $-b\leqslant y\leqslant b$, we found that

$$\begin{aligned}&i\sum_{n=0}^{\infty}\{B_ne^{-i\nu_nL}-C_ne^{i\nu_nL}\}\nu_n\int_{-b}^{b}Y_m(y)Y_n(y)dy=\\ &i\int_{-a}^{a}Y_m(y)dy-i\sum_{n=0}^{\infty}A_n\eta_n\int_{-a}^{a}\cos\{\frac{n\pi}{2a}(y+a)\}Y_m(y)dy\\ &-\frac{i}{\xi}\sum_{n=0}^{\infty}\{B_ne^{-i\nu_nL}+C_ne^{i\nu_nL}\}\int_{a}^{b}Y_n(y)Y_m(y)dy\\ &-\frac{i}{\xi}\sum_{n=0}^{\infty}\{B_ne^{-i\nu_nL}+C_ne^{i\nu_nL}\}\int_{-b}^{-a}Y_n(y)Y_m(y)dy.\end{aligned}\tag{4.63}$$

On using (3.49) and (3.50) into (4.63), we have

$$\begin{aligned}&B_me^{-i\nu_mL}-C_me^{i\nu_mL}=\frac{R_{0m}}{E_m\nu_m}-\frac{1}{E_m\nu_m}\sum_{n=0}^{\infty}A_n\eta_nR_{nm}-\\ &\frac{1}{E_m\nu_m\xi}\sum_{n=0}^{\infty}\{B_ne^{-i\nu_nL}+C_ne^{i\nu_nL}\}P_{mn}-\frac{1}{E_m\nu_m\xi}\sum_{n=0}^{\infty}\{B_ne^{-i\nu_nL}+C_ne^{i\nu_nL}\}Q_{mn}.\end{aligned}\tag{4.64}$$

By using (4.12) and (4.13) into the condition of normal velocity (4.59), we get

$$
\begin{aligned}
& i\sum_{n=0}^{\infty}\{B_n - C_n\}\nu_n Y_n(y) = \\
& \begin{cases}
\frac{i}{\xi}\sum_{n=0}^{\infty}\{B_n + C_n\}Y_n(y), & a \leqslant y \leqslant b, \\
i\sum_{n=0}^{\infty}\{D_n e^{-i\eta_n L} - E_n e^{i\eta_n L}\}\eta_n \cos\{\frac{n\pi}{2a}(y+a)\}, & -a \leqslant y \leqslant a, \\
\frac{i}{\xi}\sum_{n=0}^{\infty}\{B_n + C_n\}Y_n(y), & -b \leqslant y \leqslant -a.
\end{cases}
\end{aligned} \tag{4.65}
$$

By multiplying (4.65) with $Y_m(y)$ and integrating with respect to y over $-b \leqslant y \leqslant b$, we obtain

$$
\begin{aligned}
& i\sum_{n=0}^{\infty}\{B_n - C_n\}\nu_n \int_{-b}^{b} Y_m(y)Y_n(y)dy \\
& = +\frac{i}{\xi}\sum_{n=0}^{\infty}\{B_n + C_n\}\int_{a}^{b} Y_m(y)Y_n(y)dy + \\
& \quad i\sum_{n=0}^{\infty}\{D_n e^{-i\eta_n L} - E_n e^{i\eta_n L}\}\eta_n \int_{-a}^{a} Y_m(y)\cos\{\frac{n\pi}{2a}(y+a)\}dy \\
& \quad +\frac{i}{\xi}\sum_{n=0}^{\infty}\{B_n + C_n\}\int_{-b}^{-a} Y_m(y)Y_n(y)dy.
\end{aligned} \tag{4.66}
$$

On using (3.49) and (3.50) into (4.66), we get

$$
\begin{aligned}
B_m - C_m &= \frac{1}{E_m\nu_m}\sum_{n=0}^{\infty}\{D_n e^{-i\eta_n L} - E_n e^{i\eta_n L}\}\eta_n R_{nm} \\
&+\frac{1}{E_m\nu_m\xi}\sum_{n=0}^{\infty}\{B_n + C_n\}P_{mn} + \frac{1}{E_m\nu_m\xi}\sum_{n=0}^{\infty}\{B_n + C_n\}Q_{mn}.
\end{aligned} \tag{4.67}
$$

On using (4.13) and (4.14) into the condition of normal velocity (4.60), we found that

$$
\begin{aligned}
&i\sum_{n=0}^{\infty}\{F_n - G_n\}\nu_n Y_n(y) = \\
&\begin{cases}
\dfrac{-i}{\xi}\sum_{n=0}^{\infty}\{F_n + G_n\}Y_n(y), & a \leqslant y \leqslant b, \\
i\sum_{n=0}^{\infty}\{D_n e^{i\eta_n L} - E_n e^{-i\eta_n L}\}\eta_n \cos\{\dfrac{n\pi}{2a}(y+a)\}, & -a \leqslant y \leqslant a, \\
\dfrac{-i}{\xi}\sum_{n=0}^{\infty}\{F_n + G_n\}Y_n(y), & -b \leqslant y \leqslant -a.
\end{cases}
\end{aligned} \tag{4.68}
$$

Now we multiply (4.68) by $Y_m(y)$ and integrate with respect to y over $-b \leqslant y \leqslant b$ to get

$$
\begin{aligned}
&i\sum_{n=0}^{\infty}\{F_n - G_n\}\nu_n \int_{-b}^{b} Y_m(y)Y_n(y)dy \\
&= \frac{-i}{\xi}\sum_{n=0}^{\infty}\{F_n + G_n\}\int_{a}^{b} Y_m(y)Y_n(y)dy + \\
&i\sum_{n=0}^{\infty}\{D_n e^{i\eta_n L} - E_n e^{-i\eta_n L}\}\eta_n \int_{-a}^{a} Y_m(y)\cos\{\frac{n\pi}{2a}(y+a)\}dy \\
&-\frac{i}{\xi}\sum_{n=0}^{\infty}\{F_n + G_n\}\int_{-b}^{-a} Y_m(y)Y_n(y)dy.
\end{aligned} \tag{4.69}
$$

On using (3.49) and (3.50) into (4.69), we obtain

$$
\begin{aligned}
F_m - G_m = &\frac{1}{E_m\nu_m}\sum_{n=0}^{\infty}\{D_n e^{i\eta_n L} - E_n e^{-i\eta_n L}\}\eta_n R_{nm} - \\
&\frac{1}{E_m\nu_m\xi}\sum_{n=0}^{\infty}\{F_n + G_n\}P_{mn} - \frac{1}{E_m\nu_m\xi}\sum_{n=0}^{\infty}\{F_n + G_n\}Q_{mn}.
\end{aligned} \tag{4.70}
$$

By using (4.14) and (4.15) into the condition of normal velocity (4.61), we found that

$$
\begin{aligned}
&i\sum_{n=0}^{\infty}\{F_n e^{i\nu_n L}-G_n e^{-i\nu_n L}\}\nu_n Y_n(y)= \\
&\begin{cases}
\frac{i}{\xi}\sum_{n=0}^{\infty}\{F_n e^{i\nu_n L}+G_n e^{-i\nu_n L}\}Y_n(y), & a\leqslant y\leqslant b,\\
+i\sum_{n=0}^{\infty}H_n\eta_n\cos\{\frac{n\pi}{2a}(y+a)\}, & -a\leqslant y\leqslant a,\\
\frac{i}{\xi}\sum_{n=0}^{\infty}\{F_n e^{i\nu_n L}+G_n e^{-i\nu_n L}\}Y_n(y), & -b\leqslant y\leqslant -a.
\end{cases}
\end{aligned}
\tag{4.71}
$$

By multiplying (4.71) with $Y_m(y)$ and integrating with respect to y over $-b\leqslant y\leqslant b$, we get

$$
\begin{aligned}
&i\sum_{n=0}^{\infty}\{F_n e^{i\nu_n L}-G_n e^{-i\nu_n L}\}\nu_n\int_{-b}^{b}Y_m(y)Y_n(y)dy\\
&=\frac{i}{\xi}\sum_{n=0}^{\infty}\{F_n e^{i\nu_n L}+G_n e^{-i\nu_n L}\}\int_{a}^{b}Y_m(y)Y_n(y)dy\\
&\qquad+i\sum_{n=0}^{\infty}H_n\eta_n\int_{-a}^{a}Y_m(y)\cos\{\frac{n\pi}{2a}(y+a)\}dy\\
&+\frac{i}{\xi}\sum_{n=0}^{\infty}\{F_n e^{i\nu_n L}+G_n e^{-i\nu_n L}\}\int_{-b}^{-a}Y_m(y)Y_n(y)dy.
\end{aligned}
\tag{4.72}
$$

On using (3.49) and (3.50) into (4.72), we obtain

$$
\begin{aligned}
&F_m e^{i\nu_m L}-G_m e^{-i\nu_m L}=\frac{1}{E_m\nu_m\xi}\sum_{n=0}^{\infty}\{F_n e^{i\nu_n L}+G_n e^{-i\nu_n L}\}P_{mn}\\
&+\frac{1}{E_m\nu_m}\sum_{n=0}^{\infty}H_n\eta_n R_{nm}+\frac{1}{E_m\nu_m\xi}\sum_{n=0}^{\infty}\{F_n e^{i\nu_n L}+G_n e^{-i\nu_n L}\}Q_{mn}.
\end{aligned}
\tag{4.73}
$$

By subtracting (4.64) and (4.73), we found

$$
\begin{aligned}
&V_m^{+}e^{-i\nu_m L}-W_m^{+}e^{i\nu_m L}=\frac{R_{0m}}{E_m\nu_m}-\frac{1}{E_m\nu_m}\sum_{n=0}^{\infty}U_n^{+}\eta_n R_{nm}\\
&-\frac{1}{E_m\nu_m\xi}\sum_{n=0}^{\infty}\{V_n^{+}e^{-i\nu_n L}+W_n^{+}e^{i\nu_n L}\}\{P_{mn}+Q_{mn}\}.
\end{aligned}
\tag{4.74}
$$

On adding (4.64) and (4.73), we have

$$V_m^- e^{-i\nu_m L} + W_m^- e^{i\nu_m L} = \frac{R_{0m}}{E_m\nu_m} - \frac{1}{E_m\nu_m}\sum_{n=0}^{\infty} U_n^- \eta_n R_{nm}$$
$$-\frac{1}{E_m\nu_m\xi}\sum_{n=0}^{\infty}\{V_n^- e^{-i\nu_n L} - W_n^- e^{i\nu_n L}\}\{P_{mn} + Q_{mn}\}. \tag{4.75}$$

Similarly by subtracting (4.67) and (4.70), we get

$$V_m^+ - W_m^+ = \frac{1}{E_m\nu_m\xi}\sum_{n=0}^{\infty}\{V_n^+ + W_n^+\}\{P_{mn} + Q_{mn}\} - \frac{2i}{E_m\nu_m}\sum_{n=0}^{\infty} Z_n^+ \sin(\eta_n L)\eta_n R_{nm}. \tag{4.76}$$

By adding (4.67) and (4.70), we obtain

$$V_m^- + W_m^- = \frac{1}{E_m\nu_m\xi}\sum_{n=0}^{\infty}\{V_n^- - W_n^-\}\{P_{mn} + Q_{mn}\} + \frac{2}{E_m\nu_m}\sum_{n=0}^{\infty} Z_n^- \cos(\eta_n L)\eta_n R_{nm}, \tag{4.77}$$

where $V_m^{\pm} = (B_m \pm G_m)$ and $W_m^{\pm} = (F_m \pm C_m)$.

In the same way we get a system of equations defined by (4.34) and (4.36), (4.74) and (4.76) with unknowns U_m^+, Z_m^+, V_m^+ and W_m^+. Also a system for unknowns U_m^-, Z_m^-, V_m^- and W_m^- is given in (4.35) and (4.37), (4.75) and (4.77). These systems are truncated and solved numerically for $U_m^{\pm}$, $Z_m^{\pm}$, $V_m^{\pm}$ and $W_m^{\pm}$. Then the model amplitudes $\{A_m, B_m, C_m, D_m, E_m, F_m, G_m, H_m\}$ are obtained from these values $U_m^{\pm}$, $Z_m^{\pm}$, $V_m^{\pm}$ and $W_m^{\pm}$.

In the next section we discuss the propagation and scattering energy flux.

4.3 Energy Flux

In this section we study about the energy flux of waveguides. As the incident and transmitted regions of chapter 3 and chapter 4 are of same shape. Thus the incoming power in R_1 and outgoing power in R_5 are written as:

$$\zeta_{ref} = \frac{1}{2} Re\left[\sum_{n=0}^{\infty} \mid A_n \mid^2 \epsilon_n \eta_n\right] \tag{4.78}$$

and

$$\zeta_{tr} = \frac{1}{2} Re \left[\sum_{n=0}^{\infty} \mid H_n \mid^2 \epsilon_n \eta_n \right], \tag{4.79}$$

where the incident power being scaled at unity. By using (4.79) and incident energy flux that is unity, equation (2.11) yields the transmission loss as

$$TL = -10 \log_{10} (\zeta_{tr}) . \tag{4.80}$$

4.4 Numerical Results and Discussion

In this section, the systems of equations achieved for rigid case (4.34)-(4.37) and (4.54)-(4.57), where for vertical lining (4.34)-(4.37) and (4.74)-(4.77) are truncated by $n = m = 0, 1, 2, \ldots, N$ terms. Then each system is solved separately for respected unknowns. Thus we get the model coefficients $\{A_n, B_n, C_n, D_n, E_n, F_n, G_n , H_n\}$, $n = 0, 1, 2..., N$ terms for rigid case and vertical lining case separately. The truncated solutions are used to reconstruct the matching conditions at interfaces. All the physical parameters of previous chapter are used.

Here for rigid vertical case the pressure and velocity graphs are shown in Figures 4.11-4.18 and 4.3-4.10 respectively. It can be seen that the pressure and velocity curves coincide. It confirms the reconstruction of matching conditions at interfaces as assumed in equations (4.18)-(4.21) and (4.38)-(4.41).

Likewise for vertical absorbing lining case the pressure and velocity graphs are shown in Figures 4.19-4.26 and 4.27-4.34 respectively. It can be seen that the pressure and velocity curves coincide. It confirms the reconstruction of matching conditions at interfaces as assumed in equations (4.18)-(4.21) and (4.58)-(4.61).

Furthermore, to insight the problems physically the transmission loss is plotted against frequency in Figures 4.35-4.38. It is noted that more transmission loss with fibrous case than perforated case is obtained.

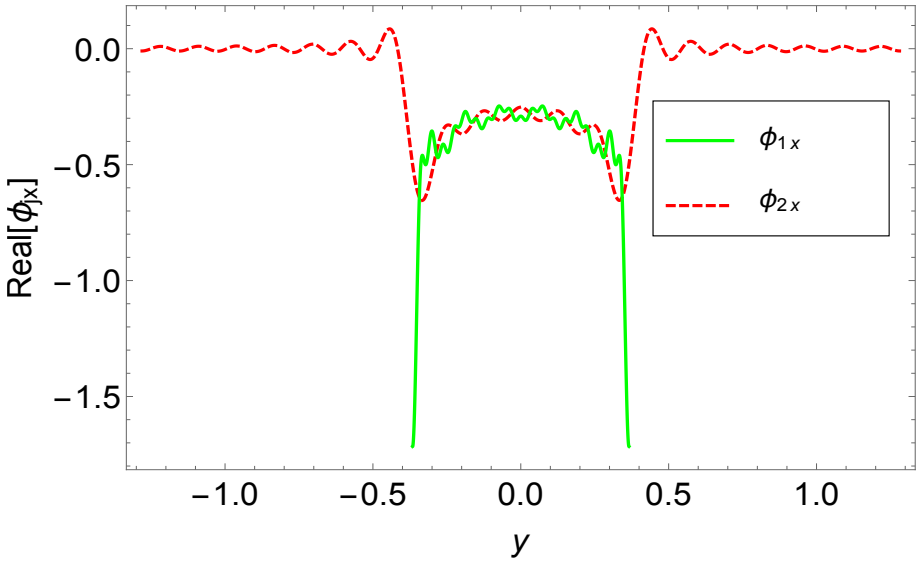

FIGURE 4.3: The real parts of velocities for rigid vertical strips at -2L.

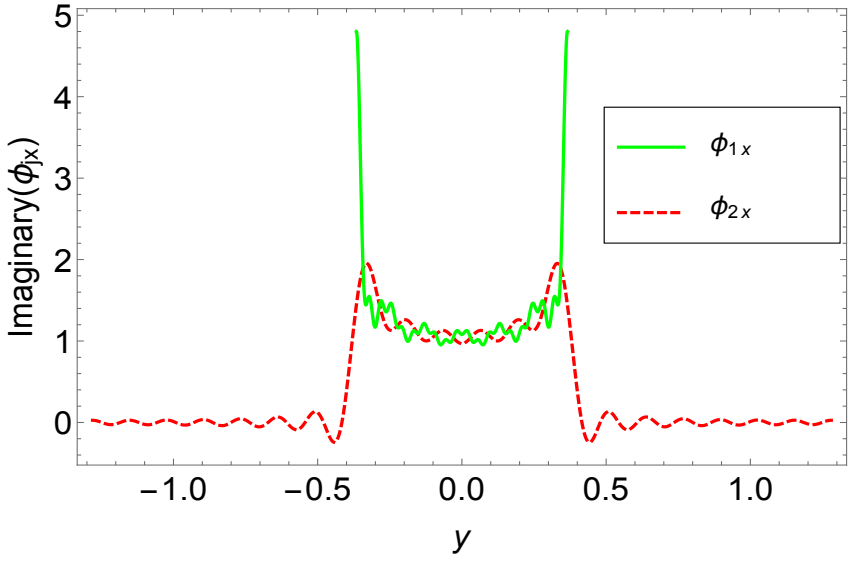

FIGURE 4.4: The imaginary parts of velocities for rigid vertical strips at -2L.

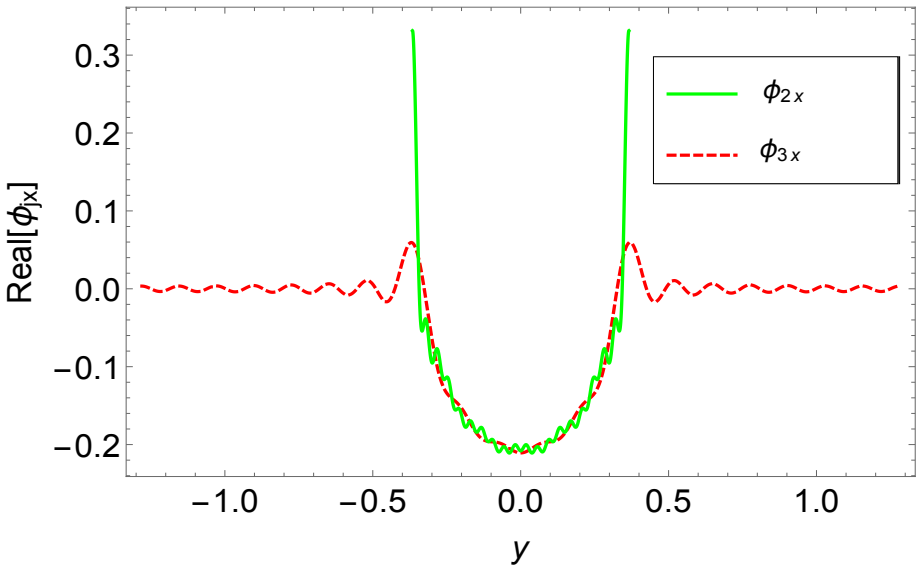

FIGURE 4.5: The real parts of velocities for rigid vertical strips at -L.

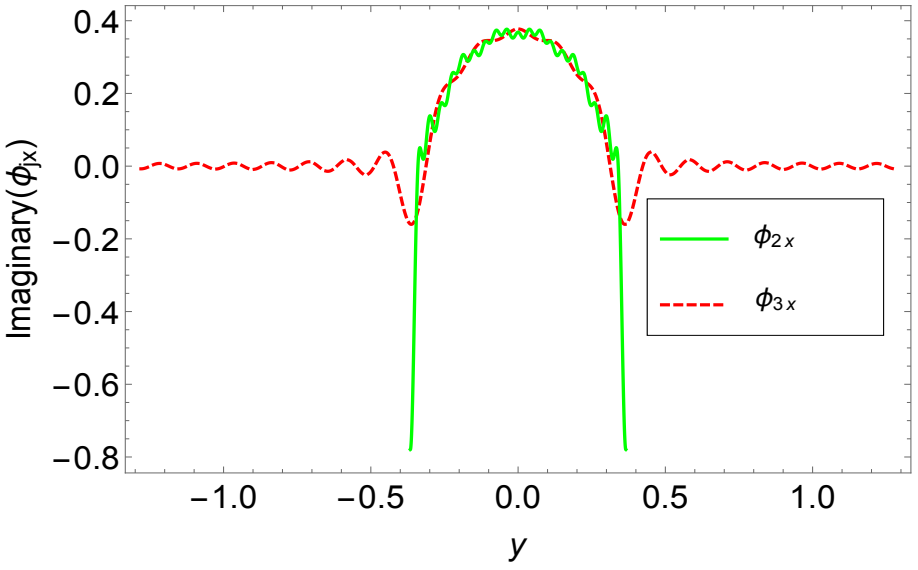

FIGURE 4.6: The imaginary parts of velocities for rigid vertical strips at -L.

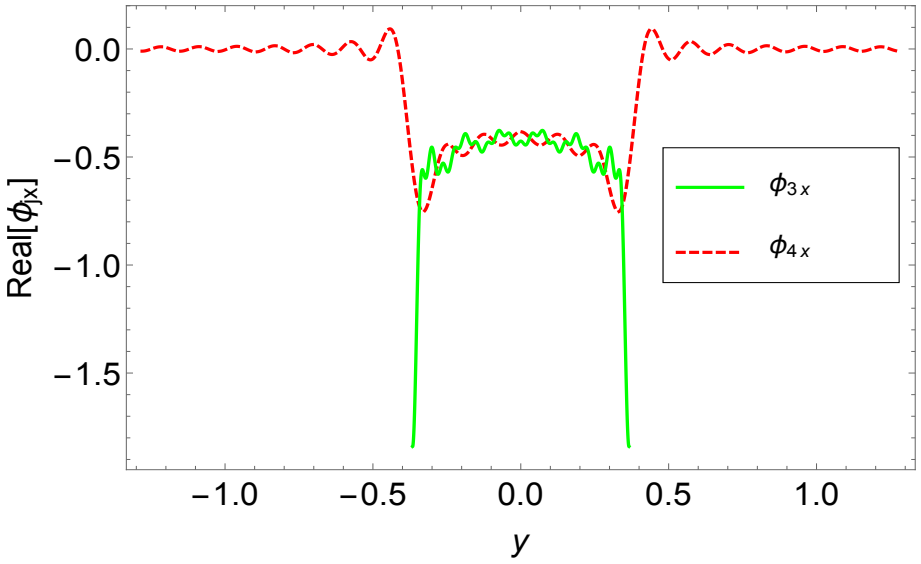

FIGURE 4.7: The real parts of velocities for rigid vertical strips at L.

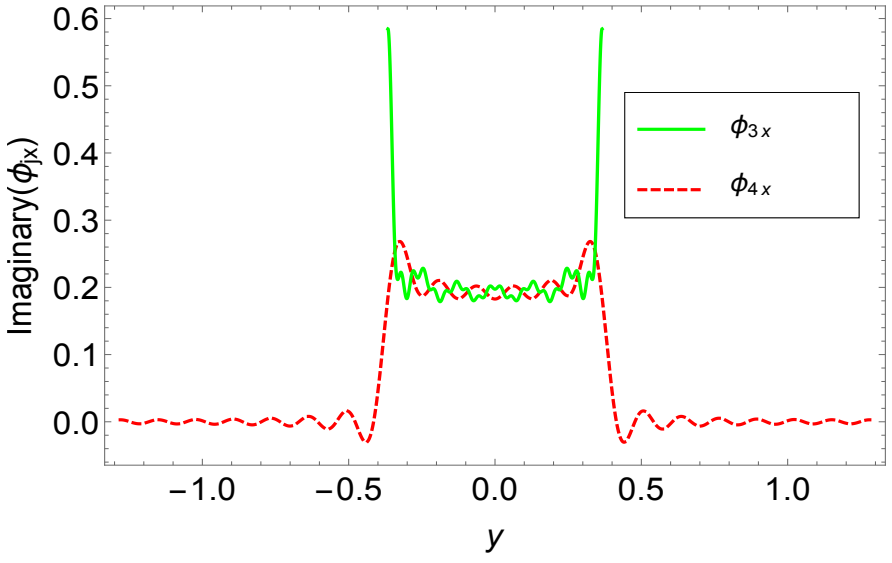

FIGURE 4.8: The imaginary parts of velocities for rigid vertical strips at L.

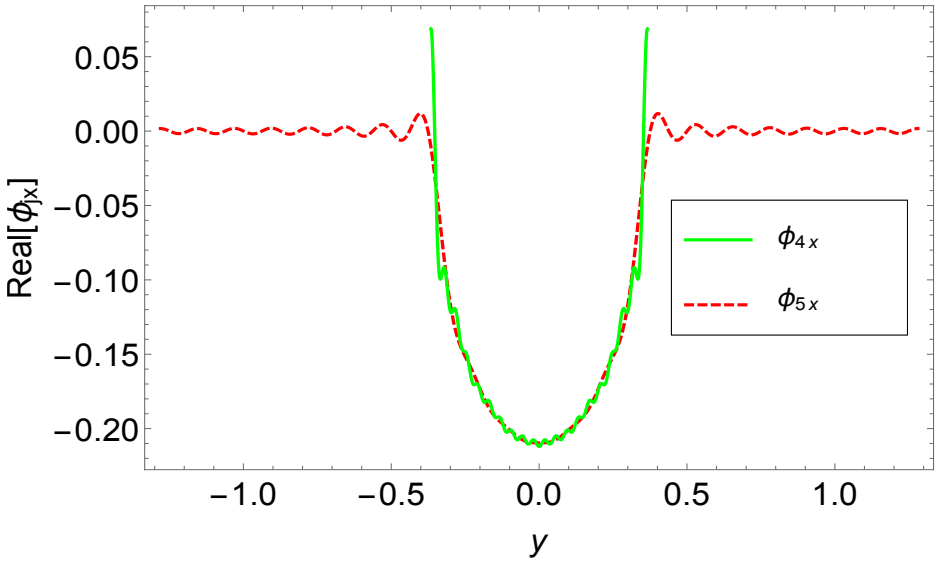

FIGURE 4.9: The real parts of velocities for rigid vertical strips at $2L$.

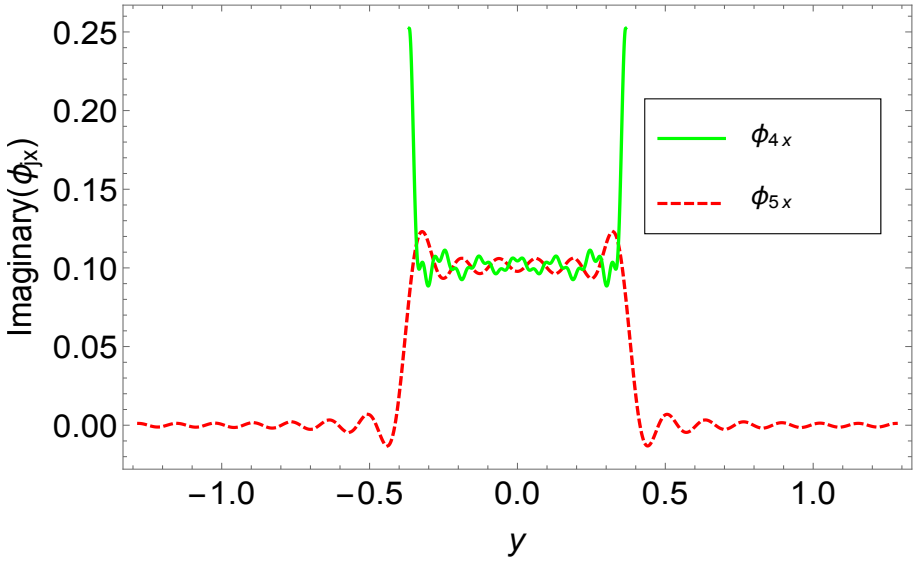

FIGURE 4.10: The imaginary parts of velocities for rigid vertical strips at $2L$.

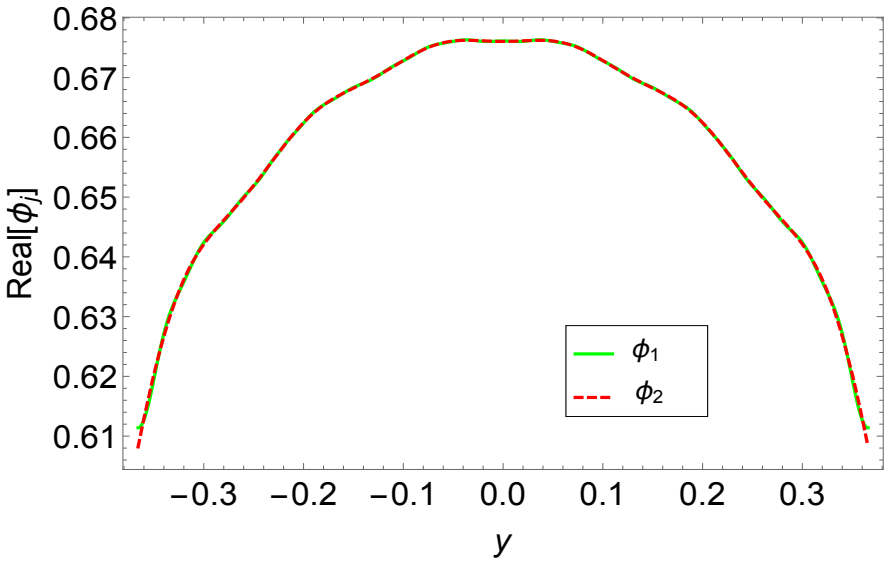

FIGURE 4.11: The real parts of pressures for rigid vertical strips at -2L.

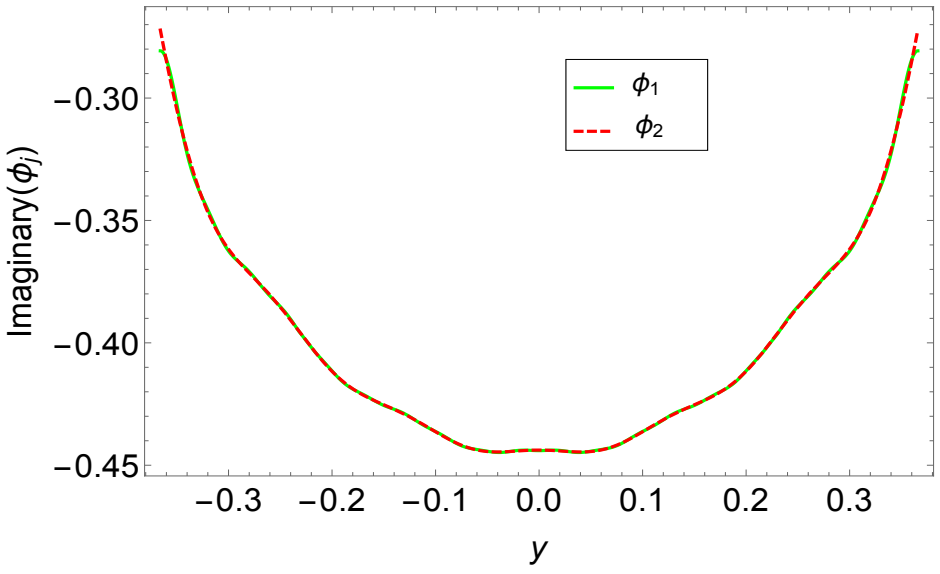

FIGURE 4.12: The imaginary parts of pressures for rigid vertical strips at -2L.

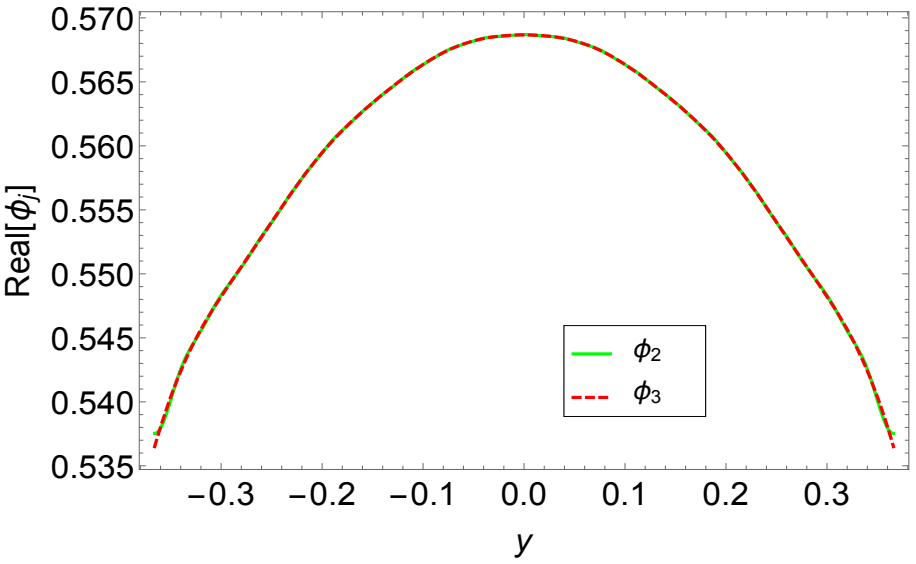

FIGURE 4.13: The real parts of pressures for rigid vertical strips at -L.

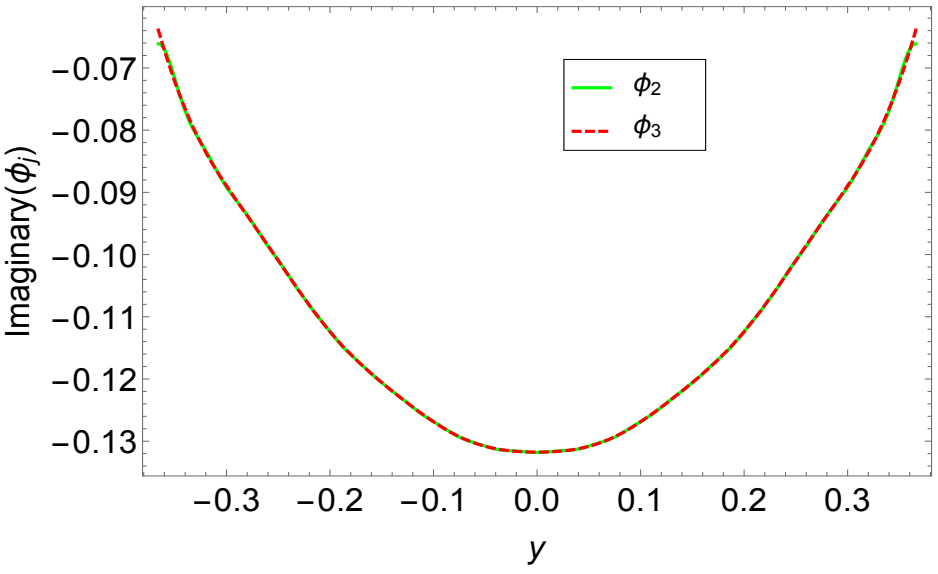

FIGURE 4.14: The imaginary parts of pressures for rigid vertical strips at -L.

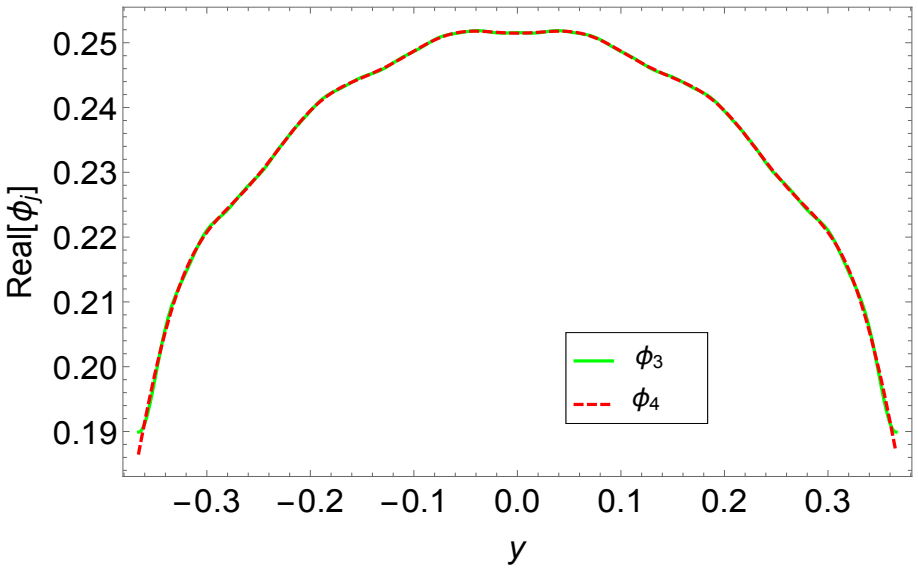

FIGURE 4.15: The real parts of pressures for rigid vertical strips at L.

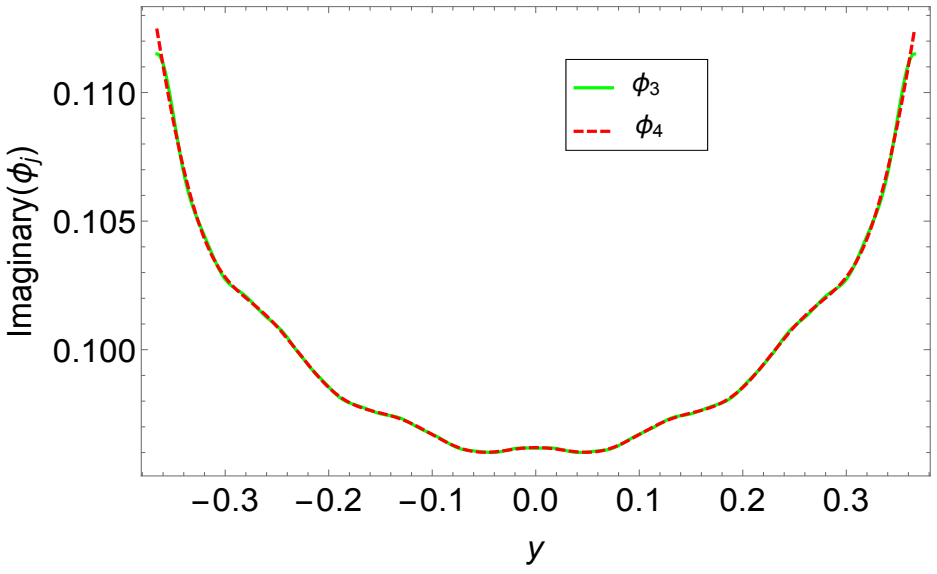

FIGURE 4.16: The imaginary parts of pressures for rigid vertical strips at L.

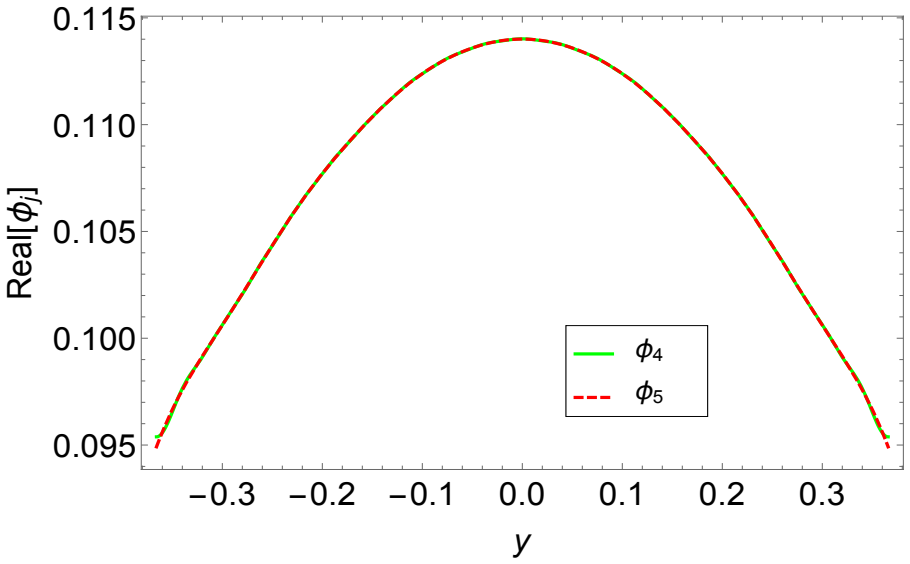

FIGURE 4.17: The real parts of pressures for rigid vertical strips at $2L$.

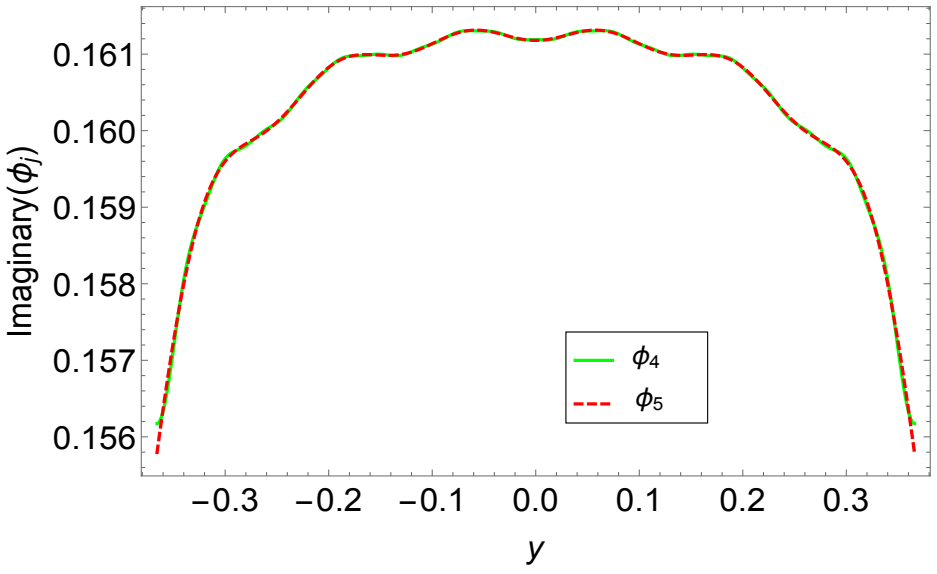

FIGURE 4.18: The imaginary parts of pressures for rigid vertical strips at $2L$.

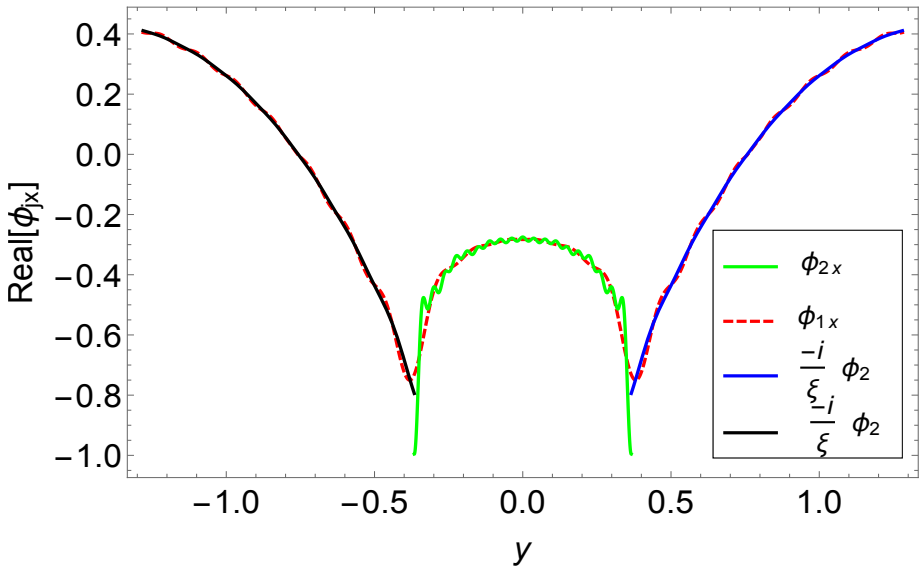

FIGURE 4.19: The real parts of velocities for vertical absorbing lining at -2L.

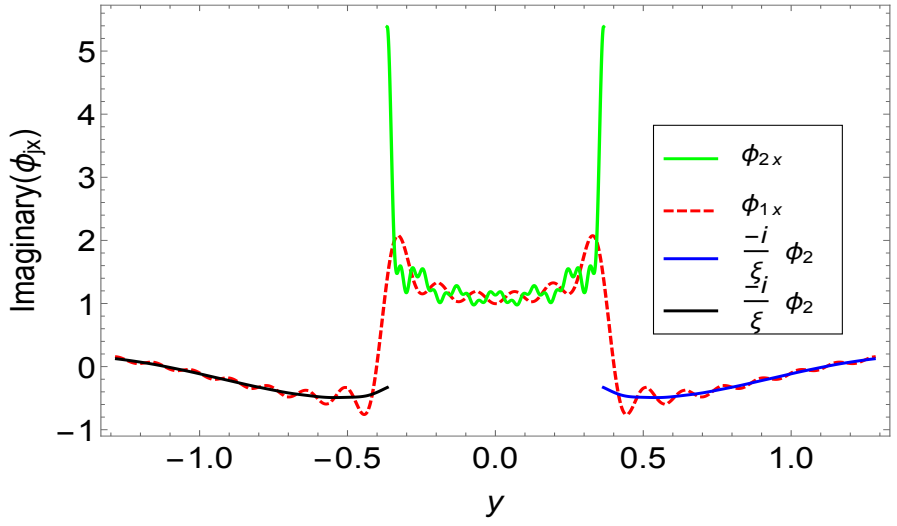

FIGURE 4.20: The imaginary parts of velocities for vertical absorbing lining at -2L.

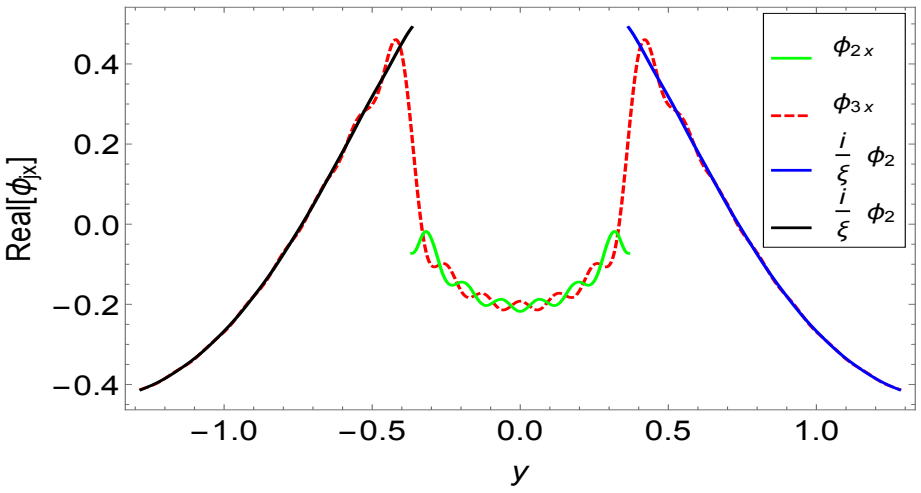

FIGURE 4.21: The real parts of velocities for vertical absorbing lining at -L.

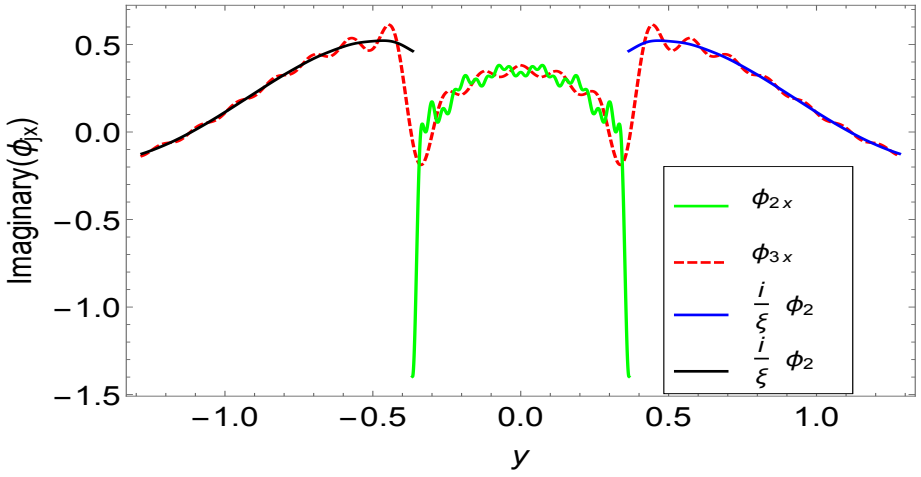

FIGURE 4.22: The imaginary parts of velocities for vertical absorbing lining at -L.

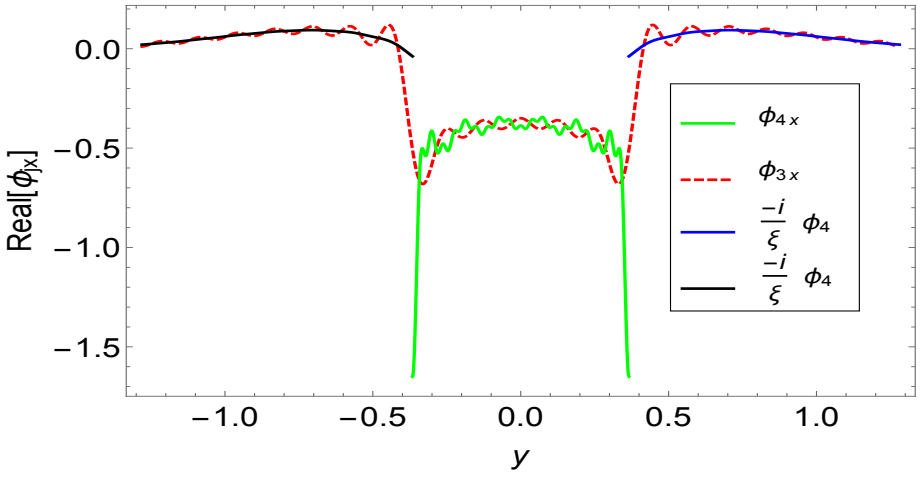

FIGURE 4.23: The real parts of velocities for vertical absorbing lining at L.

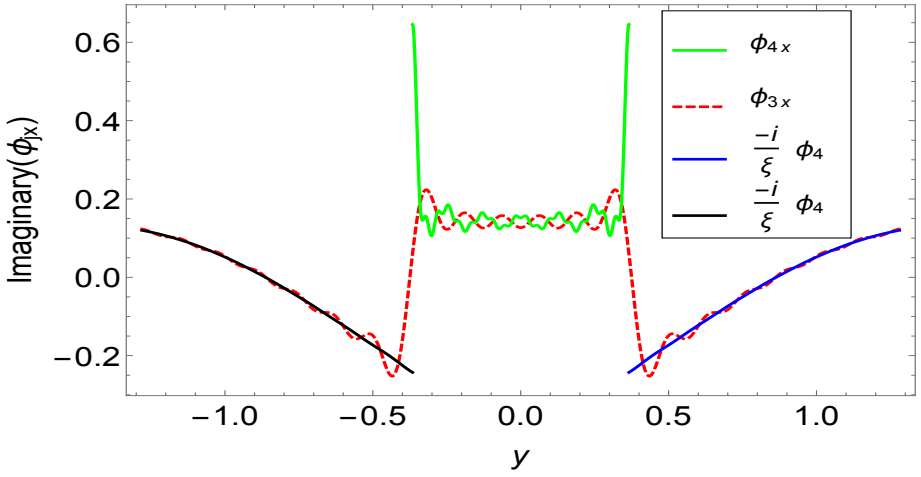

FIGURE 4.24: The imaginary parts of velocities for vertical absorbing lining at L.

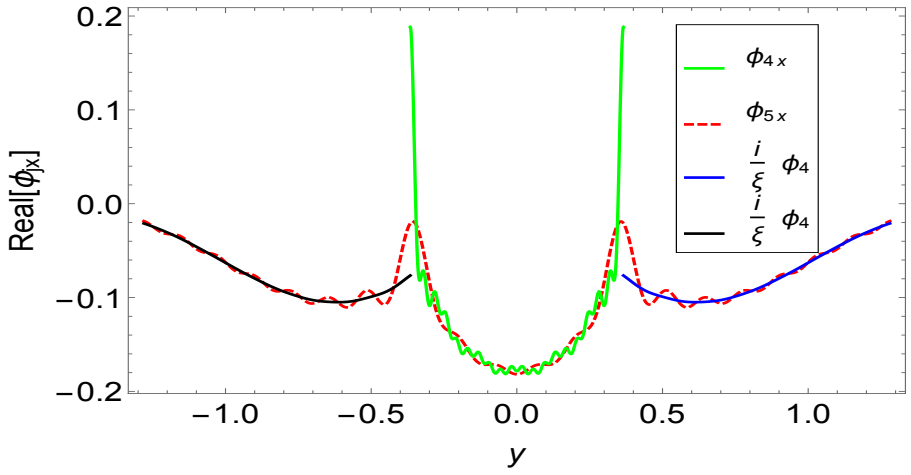

FIGURE 4.25: The real parts of velocities for vertical absorbing lining at $2L$.

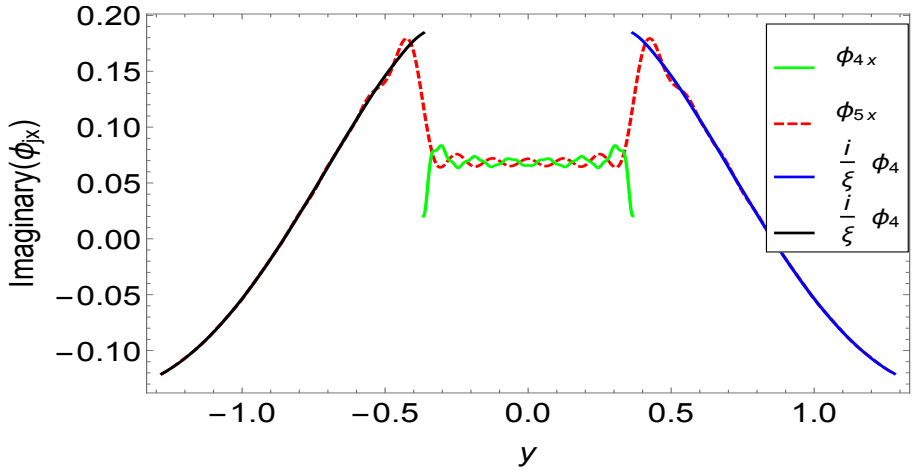

FIGURE 4.26: The imaginary parts of velocities for vertical absorbing lining at $2L$.

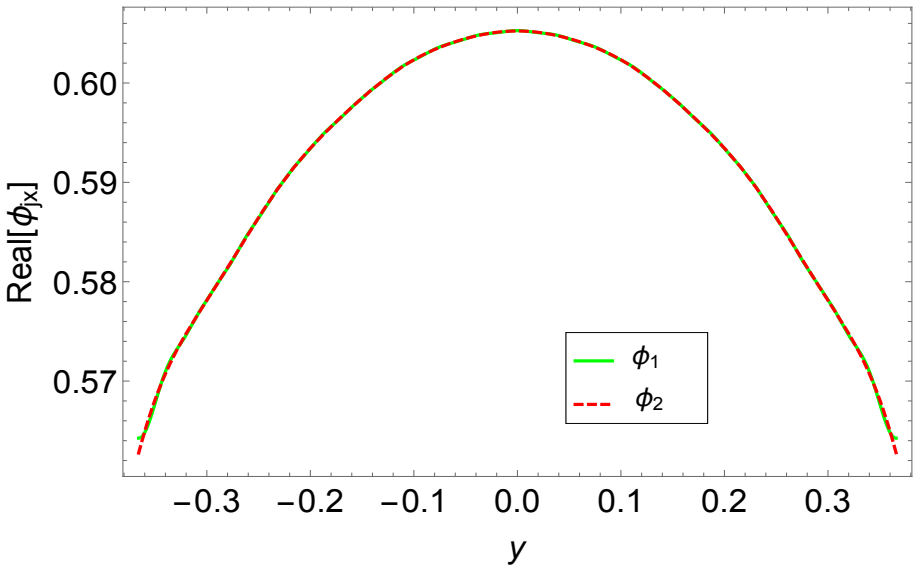

FIGURE 4.27: The real parts of pressures for vertical absorbing lining at -2L.

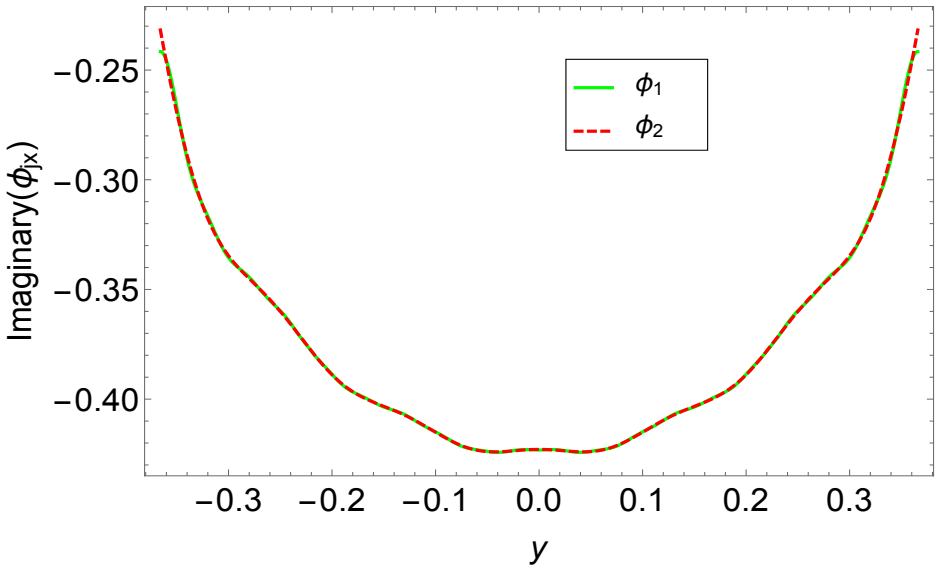

FIGURE 4.28: The imaginary parts of pressures for vertical absorbing lining at -2L.

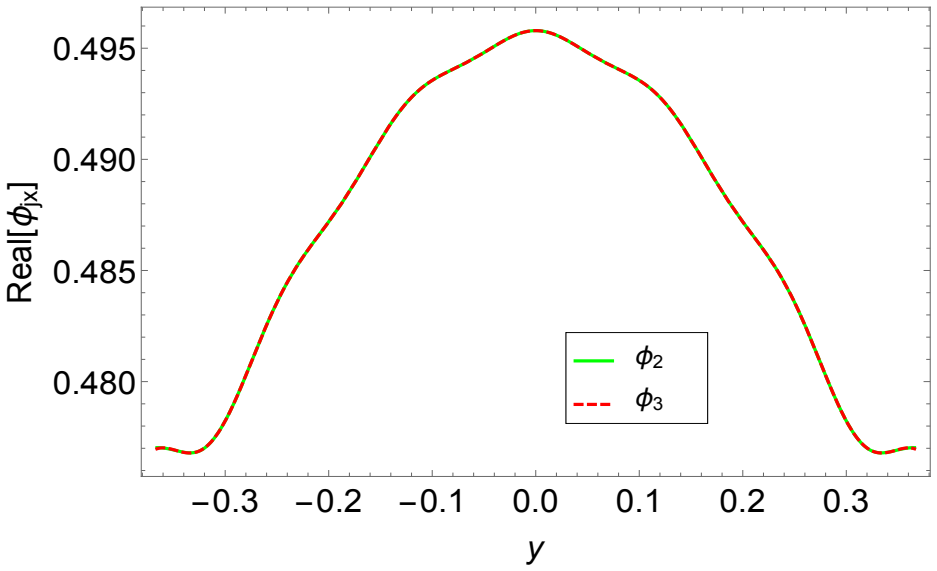

FIGURE 4.29: The real parts of pressures for vertical absorbing lining at -L.

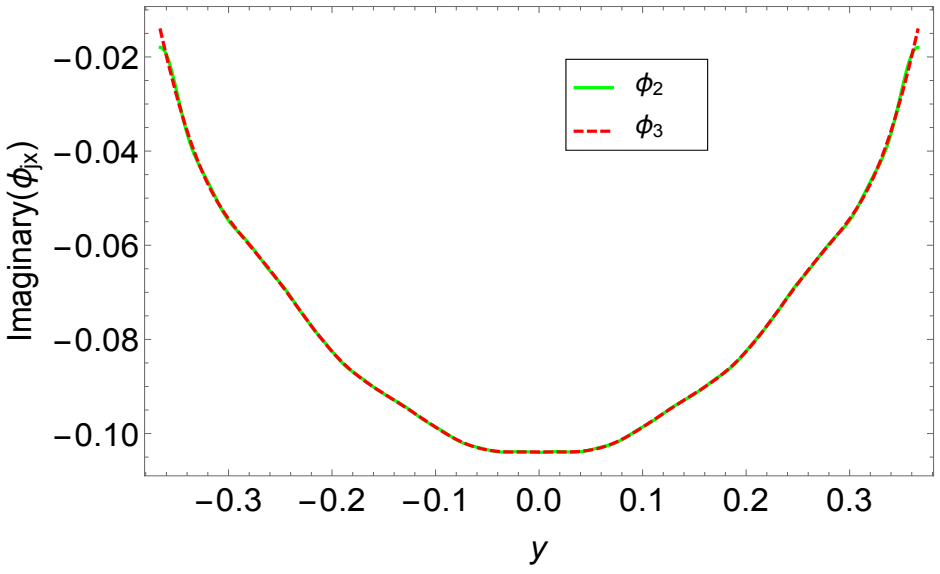

FIGURE 4.30: The imaginary parts of pressures for vertical absorbing lining at -L.

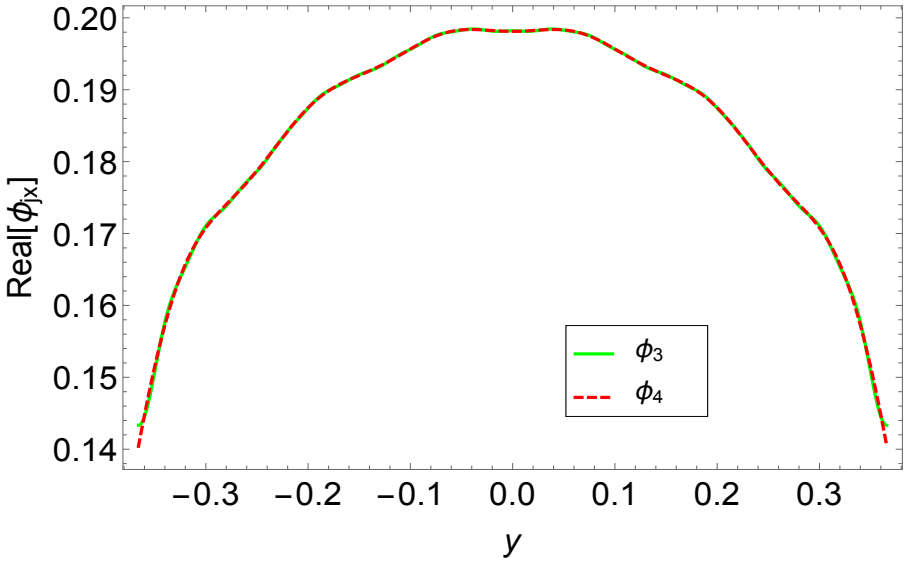

FIGURE 4.31: The real parts of pressures for vertical absorbing lining at L.

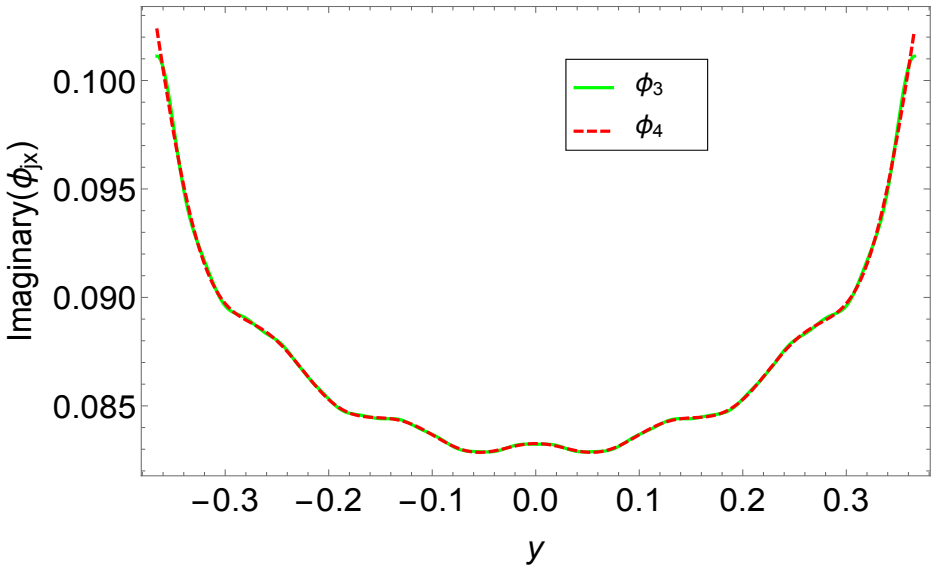

FIGURE 4.32: The imaginary parts of pressures for vertical absorbing lining at L.

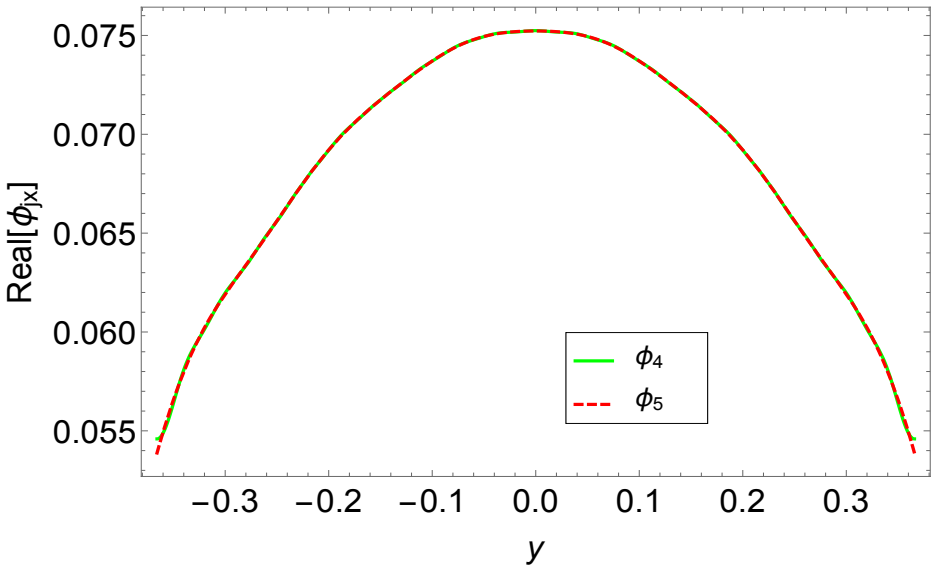

FIGURE 4.33: The real parts of pressures for vertical absorbing lining at $2L$.

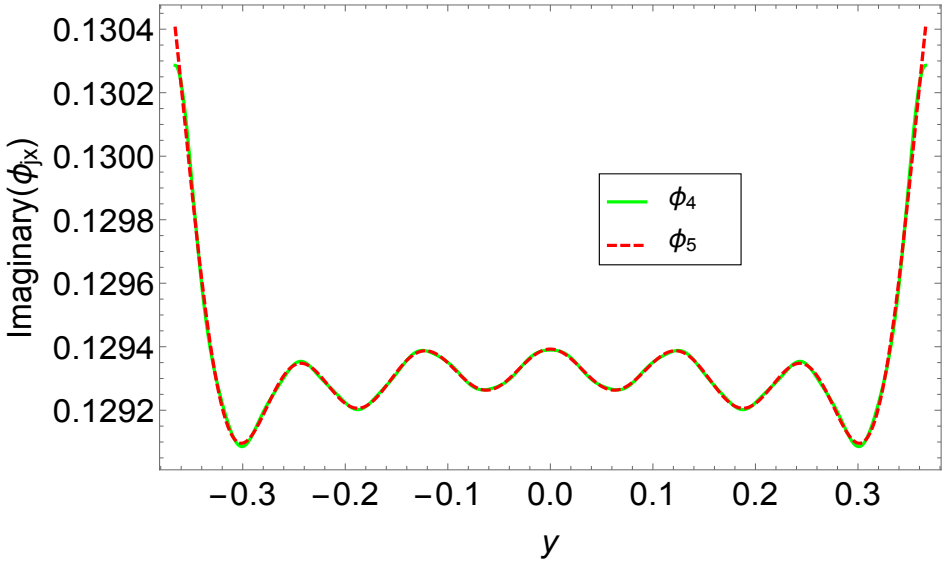

FIGURE 4.34: The imaginary parts of pressures for vertical absorbing lining at $2L$.

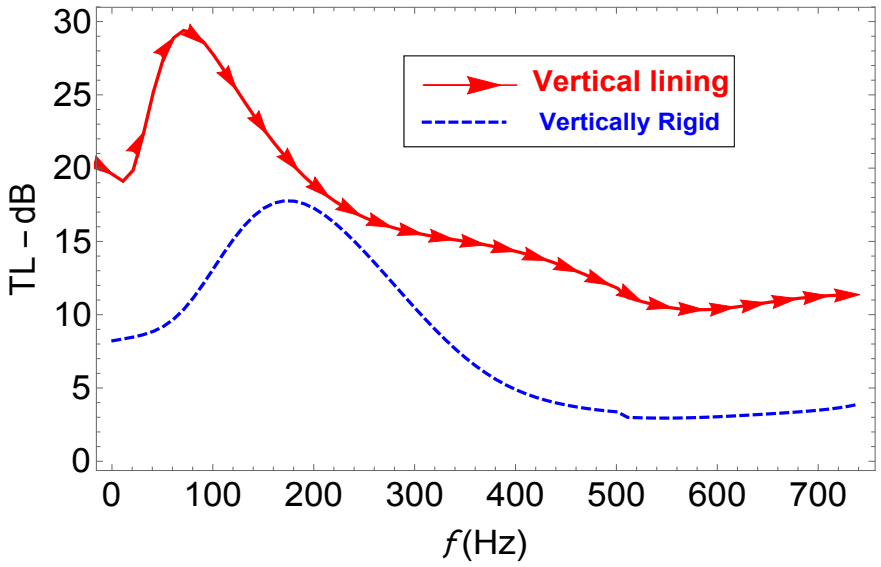

FIGURE 4.35: Transmission loss against frequency for rigid vertical and absorbing lining with $\xi = 0.5$ and $\eta = 0.5$.

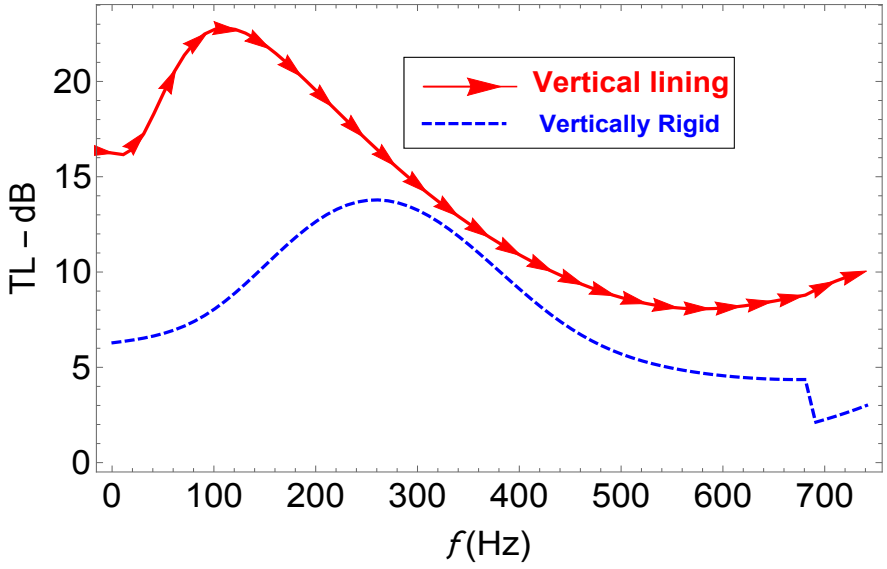

FIGURE 4.36: Transmission loss against frequency for rigid vertical and absorbing lining with $\xi = 1$ and $\eta = 0.5$.

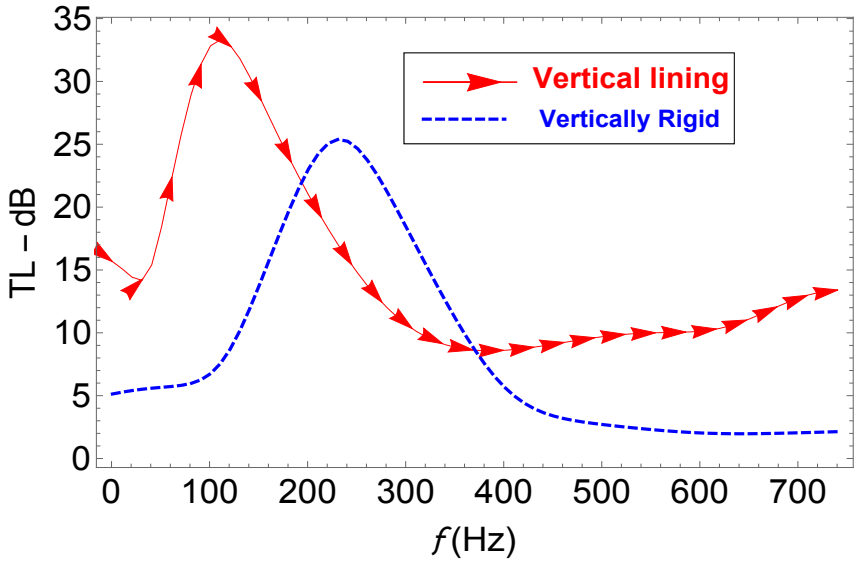

FIGURE 4.37: Transmission loss against frequency for rigid vertical and absorbing lining with $\xi = 0.5$ and $\eta = 1$.

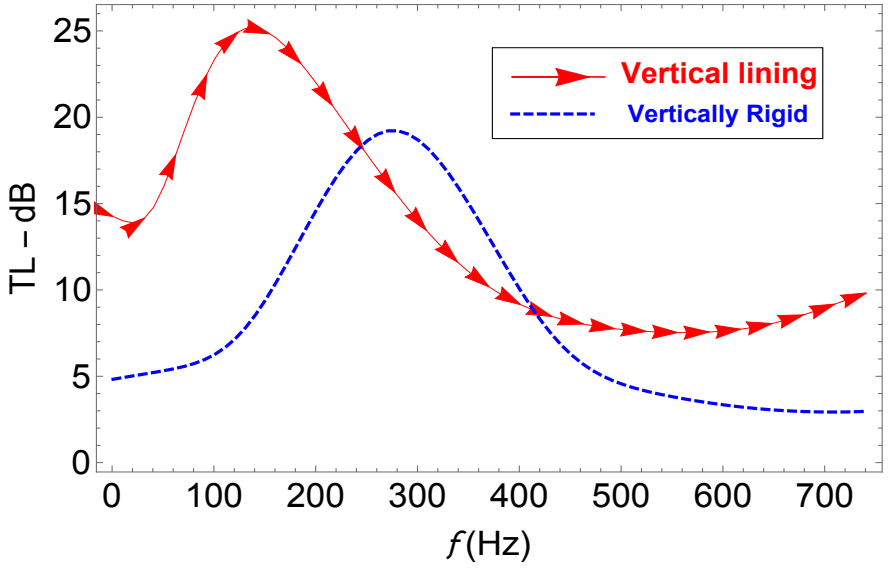

FIGURE 4.38: Transmission loss against frequency for rigid vertical and absorbing lining with $\xi = 1$ and $\eta = 1$.

Chapter 5

Discussion and Conclusion

In this thesis, we have investigated the acoustic wave scattering in waveguides including single and double expansion chambers. The inside properties of the chambers are varied. Two physical problems have been discussed in the thesis. All the problems are governed by Helmholtz equation along with rigid and/or impedance type boundary conditions. The Mode Matching technique has been applied to solve the governing boundary value problems.

The thesis contains five chapters in which Chapter 1 and Chapter 2 include introduction and basic terminologies regarding the work of Chapter 3 and Chapter 4.

In Chapter 3, the attenuation with single expansion chamber is studied. The horizontal boundaries of the chamber are lined with porous material. However, for the vertical walls of the chamber two cases are considered.

In first case the boundary value problem is solved with rigid vertical walls of the chamber whilst in later case the rigid vertical walls are replaced with absorbing lining.

In Chapter 4, the attenuation performance with two expansion chambers is discussed. Again the governing boundary value problems are splitted into two cases. First case include the two horizontally lined chambers with rigid vertical walls of the chambers whilst in the second case the rigid vertical walls are replaced with absorbing linings. The Mode Matching solution of the problems is explained in

Chapter 3 and Chapter 4. For each case the eigenfunction expansion form of solution is obtained. To discuss the problem physically the truncated form is used. First matching conditions are reconstructed to confirm the accuracy of formed truncated solutions. From the matching of pressures and velocities curves at interfaces, the truncated solution has been verified for each case.

Then the transmission loss are plotted against frequency to insight the problems physically. It is found that more transmission loss with fully lined cases than rigid vertical cases is obtained for single as well as double expansion chambers. Furthermore the properties of linings are changed. It is noted that more transmission loss with fibrous case than perforated case is obtained. Thus more attenuation performance with fibrous case and for double lined expansion chambers is observed.

Bibliography

[1] K. Peat, "The acoustical impedance at the junction of an extended inlet or outlet duct," *Journal of sound and vibration*, vol. 150, no. 1, pp. 101–110, 1991.

[2] M. U. Hassan and A. D. Rawlins, "Sound radiation in a planar trifurcated lined duct," *Wave Motion*, vol. 29, no. 2, pp. 157–174, 1999.

[3] A. D. Rawlins, "Radiation of sound from an unflanged rigid cylindrical duct with an acoustically absorbing internal surface," *Proceedings of the Royal Society of London. A. Mathematical and Physical Sciences*, vol. 361, no. 1704, pp. 65–91, 1978.

[4] A. D. Rawlins, "Wave propagation in a bifurcated impedance-lined cylindrical waveguide," *Journal of Engineering Mathematics*, vol. 59, no. 4, pp. 419–435, 2007.

[5] M. Ayub, M. Ramzan, and A. Mann, "Acoustic diffraction by an oscillating strip," *Applied Mathematics and Computation*, vol. 214, no. 1, pp. 201–209, 2009.

[6] M. Ayub, M. Tiwana, and A. Mann, "Acoustic diffraction in a trifurcated waveguide with mean flow," *Communications in Nonlinear Science and Numerical Simulation*, vol. 15, no. 12, pp. 3939–3949, 2010.

[7] M. Ayub, M. Ramzan, and A. Mann, "Line source and point source diffraction by a reactive step," *Journal of Modern Optics*, vol. 56, no. 7, pp. 893–902, 2009.

[8] L. Huang, "Broadband sound reflection by plates covering side-branch cavities in a duct," *the Journal of the Acoustical Society of America*, vol. 119, no. 5, pp. 2628–2638, 2006.

[9] Y. Choy and L. Huang, "Effect of flow on the drumlike silencer," *The Journal of the Acoustical Society of America*, vol. 118, no. 5, pp. 3077–3085, 2005.

[10] J. B. Lawrie, "Comments on a class of orthogonality relations relevant to fluid-structure interaction," *Meccanica*, vol. 47, no. 3, pp. 783–788, 2012.

[11] L. Huang, "Modal analysis of a drumlike silencer," *the Journal of the Acoustical Society of America*, vol. 112, no. 5, pp. 2014–2025, 2002.

[12] D. P. Warren, J. B. Lawrie, and I. M. Mohamed, "Acoustic scattering in waveguides that are discontinuous in geometry and material property," *Wave Motion*, vol. 36, no. 2, pp. 119–142, 2002.

[13] R. Nawaz and J. B. Lawrie, "Scattering of a fluid-structure coupled wave at a flanged junction between two flexible waveguides," *The Journal of the Acoustical Society of America*, vol. 134, no. 3, pp. 1939–1949, 2013.

[14] R. Nawaz, M. Afzal, and M. Ayub, "Acoustic propagation in two-dimensional waveguide for membrane bounded ducts," *Communications in Nonlinear Science and Numerical Simulation*, vol. 20, no. 2, pp. 421–433, 2015.

[15] M. Afzal, M. Ayub, R. Nawaz, and A. Wahab, "Mode-matching solution of a scattering problem in flexible waveguide with abrupt geometric changes," *Imaging, Multi-scale and High Contrast Partial Differential Equations*, vol. 660, pp. 113–129, 2016.

[16] M. Afzal, R. Nawaz, and A. Ullah, "Attenuation of dissipative device involving coupled wave scattering and change in material properties," *Applied Mathematics and Computation*, vol. 290, pp. 154–163, 2016.

[17] J. U. Satti, M. Afzal, and R. Nawaz, "Scattering analysis of a partitioned wave-bearing cavity containing different material properties," *Physica Scripta*, vol. 94, no. 11, pp. 115–223, 2019.

[18] T. Nawaz, M. Afzal, and R. Nawaz, "The scattering analysis of trifurcated waveguide involving structural discontinuities," *Advances in Mechanical Engineering*, vol. 11, no. 7, pp. 1–10, 2019.

[19] S. Shafique, M. Afzal, and R. Nawaz, "On mode-matching analysis of fluid-structure coupled wave scattering between two flexible waveguides," *Canadian Journal of Physics*, vol. 95, no. 6, pp. 581–589, 2017.

[20] J. B. Lawrie and M. Afzal, "Acoustic scattering in a waveguide with a height discontinuity bridged by a membrane: a tailored galerkin approach," *Journal of Engineering Mathematics*, vol. 105, no. 1, pp. 99–115, 2017.

[21] M. U. Hassan, M. Naz, and R. Nawaz, "Reflected field analysis of soft–hard pentafurcated waveguide," *Advances in Mechanical Engineering*, vol. 9, no. 5, pp. 1–11, 2017.

[22] M. H. Meylan, M. U. Hassan, A. Bashir, and M. Sumbul, "Mode matching analysis for wave scattering in triple and pentafurcated spaced ducts," *Mathematical Methods in the Applied Sciences*, vol. 39, no. 11, pp. 3043–3057, 2016.

[23] M. H. Meylan, M. U. Hassan, and A. Bashir, "Extraordinary acoustic transmission, symmetry, blaschke products and resonators," *Wave Motion*, vol. 74, pp. 105–123, 2017.

[24] A. Demır and A. Büyükaksoy, "Transmission of sound waves in a cylindrical duct with an acoustically lined muffler," *International journal of engineering science*, vol. 41, no. 20, pp. 2411–2427, 2003.

[25] M. Afzal, R. Nawaz, M. Ayub, and A. Wahab, "Acoustic scattering in flexible waveguide involving step discontinuity," *PloS one*, vol. 9, no. 8, p. e103807, 2014.

[26] P. M. Morse, "The transmission of sound inside pipes," *The Journal of the Acoustical Society of America*, vol. 11, no. 2, pp. 205–210, 1939.